Montclair State University

Montclair State University Digital Commons

Theses, Dissertations and Culminating Projects

5-2010

Ice Sheet Dynamics of the Past 17 Myr in Southern McMurdo Sound, Antarctica: A Heavy Mineral Analysis

Daniel William Hauptvogel

Follow this and additional works at: https://digitalcommons.montclair.edu/etd

Part of the Earth Sciences Commons, and the Environmental Sciences Commons

MONTCLAIR STATE UNIVERSITY

Ice Sheet Dynamics of the Past 17 Myr in Southern McMurdo Sound, Antarctica: A Heavy Mineral Analysis

By

Daniel William Hauptvogel

A Master's Thesis Submitted to the Faculty of

Montclair State University

In Partial Fulfillment of the Requirements

For the Degree of

Master of Science

May 2010

School College of Science and Mathematics

Department Earth & Environmental Studies

[redacted]

Dean Dr. Robert Prezant

5/5/2010

Date

Thesis Committee:

[redacted]

Thesis Sponsor Dr. Sandra Passchier

[redacted]

Committee Member Dr. Stefanie A. Brachfeld

[redacted]

Committee Member Dr. Matthew L. Gorring

[redacted]

Department Chair Dr. Duke U. Ophori

Abstract

The ANtarctic Geologic DRILLing program (ANDRILL) drilled a sediment core from a sea ice platform in the Ross Sea in southern McMurdo Sound (SMS), Antarctica, in late 2007. The core site is located just to the east of the Transantarctic Mountains (TAM) along the western margin of a half graben and is a site of heavy sedimentation from the TAM, the East Antarctic Ice Sheet (EAIS), the McMurdo Volcanic Group (MVG), and the West Antarctic Ice Sheet (WAIS) and Ross Ice Shelf. The upper 650 m of the core were analyzed for heavy minerals in order to interpret ice sheet drainage patterns and dynamics of the past 17 Myr. Grain mounts of the fine sand sized (63-250 μm) heavy mineral fraction of 23 intervals were created and approximately 300 grains were identified per slide. The data represents a major change in sediment provenance and indicates the Middle Miocene Climate Transition (MMCT), which was a cooling period 13.8 – 14.2 Ma. The period before the MMCT is represented by a invariant assemblage of heavy minerals in the interval 300 – 650 mbsf (15 – 17 Ma), especially static 350 – 550 mbsf, with a provenance of the Koettlitz and Ferrar Glaciers. This suggests a distal ice sheet relative to the SMS core site that is not providing any influence. Between 240 and 300 (13.8 – 15 Ma) mbsf, a change in provenance from local TAM to MVG and southern TAM occurred and mineral assemblages representing these source rocks are more abundant in the upper 240 m. This suggests a cooler environment in which the WAIS is expanding and forces transport and deposition of sediment by the EAIS from further south. This correlates well with clast provenance, wholerock geochemical data, and stratigraphic interpretations performed by other SMS team members.

ICE SHEET DYNAMICS OF THE PAST 17 MYR IN SOUTHERN MCMURDO SOUND, ANTARCTICA: A HEAVY MINERAL ANALYSIS

A THESIS

Submitted in partial fulfillment of the requirements

For the degree of Masters of Science

by

Daniel William Hauptvogel

Montclair State University

Montclair, NJ

May 2010

Copyright © 2010 by *Daniel William Hauptvogel.* All rights reserved.

Acknowledgements

I would like to thank my thesis advisor Sandra Passchier for the opportunity to work on this project and for all of her help and guidance throughout my undergraduate and graduate career at Montclair State University. I also want to thank my thesis committee members, Matthew Gorring and Stefanie Brachfeld, for their advice and support. I would like to thank the persons involved in the ANDRILL program for providing funds for this research and the collaboration over the past few years. I especially would like to thank my high school chemistry and physics teacher, Joseph Fusco, for really introducing the world of science to me. I would like to thank my parents for all of their support throughout my studies. To all of my friends at MSU, thanks for the fun and support during my time there. I especially want to thank my wonderful girlfriend, Christine, for all of her love and support.

Table of Contents **Page**

1. Introduction of Southern McMurdo Sound and the AND-2A Core

1.1 Introduction 1
1.2 Heavy Minerals 2
1.3 ANDRILL SMS Project
1.3.1 Introduction to ANDRILL 3
1.3.2 The SMS Project and Core Location 3
1.3.3 The SMS Core 4
1.4 Regional Geology 5
1.5 Glacial History 6

2. Methods

2.1 Heavy Mineral Separation 8
2.2 Petrographic Microscope Preparation 10
2.3 SEM/EDS Preparation 11

3. Results

3.1 Petrographic Results 13
3.2 SEM/EDS Results 16

4. Discussion

4.1 Mineral Source Regions 18
4.2 Possible Sources of Heavy Minerals in the Upper ~650 m of AND-2A 18
4.3 Downcore Provenance Distribution of the Upper ~650 m of AND-2A 22
4.4 Middle Miocene Glacial History 26
4.5 Comparison to SMS Team Findings 27

5. Conclusion 30

6. References 33

7. Appendix 38

8. Figures 40

9. Tables 65

List of Figures

Page

Figure 1 – (a) Location of McMurdo Sound in western Ross Sea adjacent to the northwestern corner of the Ross Ice Shelf and the Transantarctic Mountains. (b) Regional geologic map of area outline in part a. (Naish et al., 2007) 40

Figure 2 – Stratigraphic column of the upper 650 m of the AND-2A core 41

Figure 3 - Geological cross-section of Southern McMurdo Sound showing seismic stratigraphy and structural geology (Naish *et al.,* 2006). 42

Figure 4 – Generalized geologic map of the of major bedrock sources in the Ross Embayment. Modified from Licht et al. (2005) from Bushnell and Craddock (1970). 43

Figure 5 – Current integrated age model of the AND-2A core (ANDRILL SMS Science Team, 2010). 44

Figure 6 – Compilation of $\delta^{18}O$ data for the Cenozoic (Zachos et al., 2008). 45

Figure 7 – Sea surface temperature (SST) and $\delta^{18}O$ showing the MMCT cooling period (Shevenell, 2004). The lower *C. mundulus* benthic foraminifer is used as a general proxy for Antarctic ice volume. 46

Figure 8 – Distribution of dominant heavy minerals. 47

Figure 9 – SEM image of titanaugite and corresponding EDS detector spectra. 48

Figure 10 - Example SEM image (upper) and spectra (lower) of kaersutite (From sample 351.02 mbsf). 49

Figure 11 - Example SEM image (upper) and spectra (lower) of garnet (From sample 240.80 mbsf). 50

Figure 12 – Examples of dolomite SEM images with corresponding EDS detector spectra. Light grey and dark grey areas of the lower image are both dolomite. 51

Figure 13 - Example SEM image (upper) and spectra (lower) of calcite (From sample 250.54 mbsf). 52

Figure 14 - Example SEM image (upper) and spectra (lower) of ilmenite (From sample 599.02 mbsf). 53

List of Figures (Continued) **Page**

Figure 15 - Example SEM image (upper) and spectra (lower) of titanite/sphene (From sample 240.80 mbsf). 54

Figure 16 – Example SEM image of a rock fragment. 562/565 – Labradorite, 563 – Titanite/sphene, 564 – Stilpnomelane? (from sample 94.00 mbsf). 55

Figure 17 – Example SEM image (upper) and spectra (lower) of volcanic Glass with hornblende inclusion (From sample 36.74 mbsf). 56

Figure 18 – Oxidized/altered, epidote, tourmaline, apatite, and garnet overlaid on a graph based on how far from the average count percentage the counts are at each depth. Oxidized/altered grains primarily do not come from a TAM source. 57

Figure 19 – Total count percentage of TAM vs. MVG 58

Figure 20 - TAM and MVG groups overlaid on a graph based on how far from the average count percentage the counts are at each depth. The MVG shows five different pulses of sediment input, denoted by the thick black lines. 59

Figure 21 – Correlation between magnetic susceptibility and MVG minerals. 60

Figure 22 – TAM minerals broken down into source rock groups. 61

Figure 23 – Possible scenarios for ice sheet drainage dependent on the size of the WAIS (Licht et al., 2005). 62

Figure 24 - Map of McMurdo Sound area showing the ANDRILL SMS and MIS drill-sites relative to exposed deposits of the Erebus Volcanic Province (Del Carlo et al., 2009). 63

Figure 25 - Paleo-glacial-flow patterns occurring in the McMurdo Sound during the late Early-Late Miocene. A) Maximum ice-sheet expansion, consistent with the Skelton-sourced domains occurring below ca. 626 mbsf. B) Interglacial setting explaining the occurrences of Skelton-sourced ice-rafted debris in the ca. 503-488 mbsf interval. C) An Antarctic ice sheet partly reduced within the Ross Embayment above 225 mbsf. D) Interglacial setting explaining the occurrences of Koettlitz-sourced ice-rafted debris above ca. 625 mbsf. E) Reconstructed glacial setting for AND-2B glacial sediments in the ca. 626-503 mbsf and ca. 488-225 mbsf intervals (from Sandroni et al., 2010). 64

List of Tables

Page

Table 1 – Sample depths chosen for heavy mineral separation and weights throughout the procedure. 65

Table 2 – Count percentages of the most common and useful heavy minerals. 66

Table 3 – Comprehensive list of heavy minerals observed and their possible provenances. FG – Ferrar Group, KG – Koettlitz Group, BSG – Beacon Supergroup, GHIC – Granite Harbour Intrusive Complex, MVG – McMurdo Volcanic Group. 67

1: Introduction to Southern McMurdo Sound and the AND-2A Core

1.1 Introduction

The ice sheets of Antarctica are an integral part of Earth's climate system. They help regulate the Earth's climate, ocean circulation, and are a major factor for changes in sea level. The ice sheets collectively hold approximately 70 m of sea level equivalent in ice and help to create the cold Antarctic bottom water that helps drive global ocean circulation.

The ANtarctic Geologic DRILLing Program (ANDRILL) drilled sediment cores from a sea ice platform in the Ross Sea in southern McMurdo Sound (SMS) in late 2007 (Figure 1). The upper 650 m of the core (Figure 2) (~17 Ma to present) was analyzed for heavy minerals, which have a density of 2.89 g/cm^3 or higher. By completing an analysis of heavy minerals from this interval and tracing them back to their sources, the recent history (Middle Miocene, 17 Ma to present) of ice sheet drainage patterns and dynamics can be determined. Reconstructing the drainage patterns to the Ross Ice Shelf and the Ross Sea can also provide insight as to where the main snow accumulation has been located in recent history.

Investigating the period of time from the Middle Miocene to recent can also give insight into glacial conditions during the Middle Miocene Climate Optimum (MMCO), which was a warming period at approximately 15-17 Ma (Lewis et al., 2007). Almost immediately following the MMCO was the Middle Miocene Climate Transition (MMCT), which was a shift into a sudden cooling at approximately 13.8-14.2 Ma (Shevenell et al., 2004). These episodes of change are essential in understanding the effects of climate on the glacial dynamics of the area. Determining these past glacial variations is an important aspect in projecting future ice flow behavior through ice-sheet modeling and can be incorporated in global climate models (Harwood et al., 2007; Pollard and DeConto, 2009).

1.2 Heavy Minerals

A heavy mineral analysis is key in tracing multiple ice events for several reasons, the primary reason being its recording capabilities. Although ice flow patterns can be derived from glacial landforms, clast orientation in tills, or striations on bedrock surfaces, they are not suitable ways to analyze a sequence of multiple ice sheet events (Passchier, 2007). In all of these features, each glacial episode removes or overprints the evidence of a former event, and therefore will only provide indication for the most recent glacial episode. Heavy mineral deposits however, keep a complete record of glacial flow paths preserved in the stratigraphy. Once the heavy minerals are deposited, the only way to remove the record is by tectonic activity (subduction) or a very large glacial advance in which loose sediment would be bulldozed away by advancing, grounded ice.

Heavy minerals are excellent source rock indicators because they are less common and more diagnostic than most light minerals (quartz, feldspars, etc). As a result, heavy minerals have become excellent tracers of glacial flows by being able to trace these minerals back to their source rocks. An area like SMS is a suitable place for a heavy mineral analysis because of the distinct surrounding rock types and half graben structure of the sedimentary basin.

1.3 ANDRILL SMS Project

1.3.1 Introduction to ANDRILL

ANDRILL is a multinational collaboration of five countries (Germany, Italy, New Zealand, the United Kingdom and the United States) with a primary goal to recover stratigraphic records from the Antarctic margin in order to develop a detailed history of paleoenvironmental changes. The first two drillings of this consortium were the McMurdo Ice Shelf (MIS) project 2006-2007 and the SMS project 2007-2008, and there are other projects currently in development.

1.3.2 The SMS Project and Core Location

The SMS project had numerous objectives to achieve during on-ice and off-ice research. These objectives included determining initial onset and history of sea ice presence and its contribution to the thermohaline ocean circulation, to test if stable cold-polar climate conditions existed for the past 15 Myr (Harwood et al., 2006), to recover a stratigraphic sequence deposited during the middle Miocene to observe the MMCO and MMCT in greater detail (Harwood et al., 2006), and many more. A continuous and detailed sediment core of the Early and Middle Miocene has not been recovered on the continental shelf of Antarctica. All objectives were pointed toward a broader scope: "(To) advance significantly our ability to bring Antarctica's role in the global picture to clearer focus" (Harwood et al., 2006).

The SMS core site is located within the Ross Sea, adjacent to the Transantarctic Mountains (TAM) front in the southern Victoria Land basin. Its exact geographical location is 77°45.488 S; 165°16.613 E. Tectonic uplift of the TAM and movement of the

West Antarctic Rift System (WARS) has formed a half graben structure in which sedimentary strata have been deposited for much of the Cenozoic (Figure 3) (Harwood et al., 2006). The SMS site is surrounded by several distinct source rocks (Figure 4) and therefore serves as an excellent indicator of environmental change. The area receives sediment supplied by outlet glaciers coming from the Transantarctic Mountains (TAM), the East Antarctic Ice Sheet (EAIS), West Antarctic Ice Sheet (WAIS) and the Ross Ice Shelf (RIS), volcanic sediment from the McMurdo Volcanic Group (MVG), and biogenic sediment generated within the Ross Sea.

1.3.3 The AND-2A SMS Core

The SMS on-ice science team recovered 1138.54 m of sediment core from an 8.5 m thick sea ice platform over 380 m of water. Of the sedimentary record recovered, diamictite was the dominant lithology. There were also volcanic and non-volcanic sandstones and conglomerates, mudrocks, and diatomites. The core was separated into 14 lithostratigraphic units that were identified during on-ice core description. The criteria used to define the lithostratigraphic units and identify changes include diamictite abundance, sandstone/mudstone abundance, volcanogenic component in lithologies, biogenic silica abundance, and abundance of conglomerate within diamictite-dominated intervals (Fielding et al., 2008, in press).

The SMS core has several possible hiatuses in the upper 300 m, which covers approximately 15 Myr in age based on the age model developed by the ANDRILL-SMS Science Team (2010) (Figure 5). Below the 300 m interval the core is of much higher resolution, only spanning about 3 Myr. This provides an excellent record of the Early-Middle Miocene, which was a primary area of interest for the ANDRILL program.

1.4 Regional Geology

Antarctica is approximately 14,200,000 km^2 in area (Anderson, 1999). It is comprised of two major continental blocks, East Antarctica and West Antarctica. The boundary between the two are the Transantarctic Mountains (TAM) which span nearly 3,500 km and have elevations just over 4,500 m (Fitzgerald, 2002). The formation of the East Antarctic craton began in the early Archean (Borg et al., 1987) and was interpreted by Black et al. (1983) to have become fully developed by the middle Proterozoic. West Antarctica, which is mainly below sea level at the present time, is much younger, forming during the Mesozoic and Cenozoic and is composed of several microplates with metamorphic and volcanic terrains (Anderson 1999, Fitzgerald, 2002).

Since rifting in the Proterozoic, the TAM have undergone repeated tectonism and transpression and subduction-related magmatism in the mid-late Cambrian (Fitzgerald, 2002). Following the Cambrian was the Ross orogeny and then uplift related to Jurassic magmatism when the dolerite sills and basaltic flows were emplaced (Fitzgerald, 2002). The present-day TAM though, are the result of three episodes of uplift occurring during the Early Cretaceous, Late Cretaceous, and early Cenozoic (Fitzgerald, 2002). Each of those events is related to the breakup of Gondwana and the separation of Antarctica from other continents as it moved to its present polar location.

The basement of the TAM is primarily composed of late Proterozoic-Cambrian amphibolite facies, metamorphic rocks of the Koettlitz Group, which are intruded by the

Cambrian-Ordivician granitoids of the Granite Harbour Intrusive Suite (GHIS) (Fitzgerald, 2002; Sandroni and Talarico, 2006). The Koettlitz Group is composed of biotite and hornblende schists, marbles, quartzites, amphibolites, and leuco- and paragneisses (Sandroni and Talarico, 2006).

This is unconformably overlain by the Beacon Supergroup which is composed of Devonian-Triassic glacial, alluvial, and shallow marine sandstones, siltstones, conglomerates and minor coal measures (Barrett, 1991; Sandroni and Talarico, 2006). The Ferrar Group dolerite sills and dykes of the Jurassic intruded the basement complex and Beacon Supergroup simultaneously with the eruption of the extrusive Kirkpatrick Basalt (Elliot, 1975). This is all followed by a 160 Ma gap in the geologic record until the Miocene volcanism of the McMurdo Volcanic Group (LeMasurier and Thomson, 1990) with the eruption of trachytic rocks 19-10 Ma and basanitic to phonolitic during the past 10 Myr (Sandroni and Talarico, 2006).

Since the glaciation of Antarctica in the Cenozoic, outlet glaciers have been providing eroded sediment to the SMS site from all of these formations. These outlet glaciers include the Koettlitz Glacier, which is closest to the drill site. Other glaciers include the Skelton and Mulock Glaciers to the south, and the Ferrar Glacier to the west as well as the possibility of sediment input from major outlet glaciers further south, such as the Shackleton, Byrd, or Beardmore Glaciers. A map showing general geology and location of major outlet glaciers is presented in Figure 4.

1.5 Glacial History

It is known that Antarctica began to form its ice sheets approximately 34 Ma around the Eocene-Oligocene boundary. Tectonic activity on the continent, such as the uplift of the TAM, and the decrease in pCO_2 strongly influenced the early Antarctic ice sheet (DeConto and Pollard, 2003; Zachos et al., 2008).

Since its formation, there have been several changes in ice sheet volume. Zachos et al., (2008) have compiled a Figure showing $\delta^{18}O$ for the past 60 Myr (Figure 6). Based on that figure, by the end of the Oligocene, climate was warming and then there was a sudden cooling and expansion of the Antarctic ice sheets into the beginning of the Miocene. Shortly thereafter was the MMCO, which was the warming period approximately 15-17 Ma (Lewis et al., 2007). This was then followed by the MMCT, which was a shift into a sudden cooling approximately 13.8-14.2 Ma identified by Shevenell et al. (2004) (Figure 7) and supported by evidence from Lewis et al. (2007). This cooling trend continued and peaked at the last glacial maximum (LGM).

In 1981 the ice sheets of Antarctica were about 80% of the volume they were during the LGM (Denton and Hughes, 1981), and may be less today with activity such as the collapse of the Larsen A and B ice shelves. The collapse of these ice shelves did not contribute to sea level rise however, it did lead to surging glaciers.

2. METHODS

2.1 Heavy Mineral Separation

The method used for heavy mineral separation followed very closely to what was described by Mange and Maurer (1992). The size fraction of heavy minerals desired for this study was 63-250 μm. Grains smaller than 63 μm would prove too small to identify with a petrographic microscope and grains larger 250 μm would be too thick to allow proper identification. In order to analyze heavy minerals of this size fraction, core samples were sieved and separated based on densities. For this research, density 2.89 g/cm^3 was used as the distinction between light and heavy minerals. Other studies have used 2.83 g/cm^3 (Polozek and Ehrmann, 1998) and 2.9 g/cm^3 (Damiano and Giorgetti, 2008) as the boundary between light and heavy minerals. The 2.89 g/cm^3 was dictated by the liquid form of the sodium polytungstate used for separation and also allows this study to be comparable to other heavy mineral studies.

Sample depths to choose from had already been preselected based on sand percentage. It was decided to start processing samples at the top of the core, because the sediment would not be as compacted and the methods of separation could be easily tested. Once the methods were sound, samples were taken approximately every 50 m through the core down to 650 m in order to develop a good representation of the core. After analyzing those samples on a petrographic microscope, additional depths were chosen for analysis between intervals where there was a distinct change in the heavy mineralogy. A total of 24 samples (Figure 8) were successfully sieved and separated using the methods described below, however sample 28.22 mbsf did not yield enough heavy minerals to obtain a representative count.

Samples were broken apart to get anywhere from 8 to 16 g of sediment and the exact starting weight was recorded (Table 1). Samples near the top of the core disaggregated fairly simply relative to deeper intervals. The primary method used for disaggregation was gentle crushing in an agate mortar and pestle, though more compacted sediments required force from a rock hammer to separate. It was imperative to avoid any sort of grinding motion at this point so that the grains themselves would not be crushed, but just separated from other grains. Grinding of the grains would have caused the minerals to lose any morphology and change size, which would ultimately skew mineral abundances in the grain counting results.

Once the samples were broken down into individual grains, they were wet sieved through a 63 μm sieve in order to remove the finer particles. The remaining sediment was dried out completely in an oven, around 60°C. The samples were then placed into a larger, dry sieve to separate particles larger than 250 μm. The remaining fine sand fraction was weighed and was used for heavy liquid separation (Table 1).

All samples were separated using a sodium polytungstate heavy liquid with a density of 2.89 g/cm^3. There were two methods of preparation of the heavy liquid, based upon availability of materials. One preparation was to use an already prepared liquid with a preset density of 2.89 g/cm^3. The second method was the use of a sodium polytungstate powder in which the density was controlled by adding or evaporating water until the proper density was reached. The formula given by the manufacturer was 1 lb of powder to 101 grams of water to create a 2.89 g/cm^3 mixture. In both cases, density was measured with a hydrometer to ensure the specifications were met.

The 63-250 μm fractions of the samples and sodium polytungstate liquid were put into 50 mL centrifuge tubes and placed in a centrifuge for 15 minutes at 3000 revolutions per minute. This ensured that heavy minerals would sink to the bottom of the tube and light minerals would float to the top. The bottom third of each tube was frozen in a beaker of dry ice in order to extract the light fraction without losing any of the heavy fraction. With the heavy fraction frozen at the bottom, the light fraction was poured over filter paper so that the sodium polytungstate liquid could be reused. Once the heavy fraction thawed, it was also washed out of the tube over filter paper. Both the light and the heavy mineral sample fractions were rinsed with water to remove any residual heavy liquid and were placed in the oven for drying. Both sets of samples were then weighed (Table 1).

2.2 Petrographic Microscope Preparation

To optically identify the heavy minerals, grains had to be mounted on microscope slides. Grains were immersed in Norland Optical Adhesive 61 (R.I. 1.56) on microscope slides and cover slips placed on top. It was important to make sure that air bubbles were kept to a minimum, as they would impede identification. The slides were placed under UV light in order for the adhesive to cure.

Grains mounts were counted using a Leica DMLP Polarizing Microscope. To ensure that the grains counted would be a representative example, 300 counts per slide were necessary. Two straight lines were drawn on the cover slip down the middle of the slides; all grains fully within those boundaries were counted. Grains that remained partially on the boundary line and outside were not counted. In some cases, an additional boundary line would have to be drawn if there were less than 300 grains within the initial set. Counts per slide ranged from approximately 290-310.

Grains were identified using several optical properties. Birefringence and extinction provided the foundation of all identification. Other properties frequently used were pleochroism, relief, cleavage, morphology, and color. Interference figures and elongation are difficult to determine from grain mounts and therefore were not used as a source of identification. In all cases, grain characteristics were compared to those of representative minerals listed in "Heavy Minerals in Colour" (Mange and Maurer, 1992).

2.3 SEM/EDS Preparation

Lucite acrylic discs, 26 mm in diameter, were used to mount grains for scanning electron microscope/energy dispersive spectrometer (SEM/EDS) analysis. Each disc had 7 to 9 holes drilled through them. After applying tape to one side of the disc, grains were handpicked under a microscope and were placed into the drilled holes. A representative selection was also used. These holes were then filled with a 2-part epoxy to set the grains in place. Once dry, the tape was removed and the disc was run through a series of polishing steps on a Buehler Minimet 1000 Grinder-Polisher. A 600 grit carbimet paperdisc and a few drops of water were first used for approximately five minutes. Then a Buehler MetaDi monocrystalline diamond suspension (6 µm in size) was used for fifty minutes in two twenty five minute intervals. The final polishing step was another diamond suspension (1µm in size) used for one hour in two thirty minute intervals.

Between each interval, the discs were inspected under a petrographic microscope to ensure polishing was successful and to determine if the discs required extra time during a particular step. The polishing was used to create a polished surface for SEM/EDS. A polished surface was needed in order to generate good quantitative data for the X-ray analysis.

Samples were analyzed on a Hitachi S-3400N Scanning Electron Microscope with a Bruker X-Ray detector. A standardless EDS analysis was used at the time of sample processing because there were technical issues with creating a standard library. Accuracy of the standardless analysis is +/- 2% for major elements. Due to beam skirting with uncoated samples in variable pressure mode, weight percent data is further skewed. Standardless analysis was tested on the USGS rock standard W-2. The results yielded accuracy within ten weight percent of the accepted data on oxides present in amounts greater than two weight percent. Though the weight percent data is imprecise, it is enough to aide in the identification of minerals that were optically similar (types of pyroxenes, amphiboles, iron oxides). It is important to recognize that in some cases the polishing steps did not reveal entire grain boundaries because of differences in height within surfaces of the grains, so morphology was not always prevalent. An appendix of numerous mineral spectra from Reed (2005) was used as the primary guide for interpreting data.

Samples were analyzed using an accelerating voltage of 15 kV and a working distance of approximately 10 mm. A 10 mm working distance is what is recommended for the Bruker X-ray detector in order to obtain maximum count rates.

3. Results

3.1 Petrographic Results

The heavy mineral fraction was generally 1% - 3% of the starting weight (Table 1). A percent count summary of the most abundant minerals is presented in table 2. Complete raw count data and percentage count data can be found in the appendix. It is clear from the results that the bulk of the mineralogy is composed of pyroxene and oxidized/altered minerals. Generally, pyroxenes and oxidized minerals composed roughly two thirds of each sample. The most abundant minerals include oxidized/altered grains, diopside, augite, enstatite, hornblende, and volcanic glass with inclusions. More uncommon minerals found were clinozoisite, garnet, apatite, biotite, tourmaline, opaques and others in even lesser quantities.

Oxidized or altered minerals were identified by the presence of a black, and sometimes brown, alteration on the surface of the grains. This prevented identification using the techniques listed earlier. It is important to understand that most of the minerals in these samples showed evidence of oxidation, but only minerals that were altered beyond recognition were classified as oxidized. Opaque grains were distinguished from oxidized minerals by their nature to remain completely black under both plain and crossed polarized light. Though the oxidized grains were black as well, small spots of color could usually be seen on the outer edges of the grains. Most of the oxidized grains are likely some member of the pyroxene or amphibole group since they are the most abundant. Some grains had a noticeably larger area of birefringence that resembled pyroxene, but they could not be identified with 100% certainty.

Clinopyroxenes are extremely difficult to differentiate under a petrographic microscope, however an attempt was made to classify them based on color. Other studies have been completed around the same region that separated clinopyroxenes by cleavage (Polozek and Ehrmann, 1998, Ehrmann and Polozek, 1999). During the counting process, most of the clinopyroxenes exhibited a prominent cleavage, especially the colorless and green grains, and therefore did not become part of a classification scheme. The brown and purple clinopyroxenes exhibited cleavage very poorly or not at all. Grains identified as diopside (diopsidic) were colorless and exhibited a large extinction angle. Their characteristic color banding under crossed polarized light and high birefringence were primarily used in identification. Augite (augitic) grains were differentiated from diopside and broken into groups based on their color, which varied from green, brown, red, and purple, and pleochroism, which was green/brown, red/brown, and red/pink. Some prismatic augite grains also exhibited hexagonal terminations at both ends of the crystal. These grains were typically the purple/dark red titanaugites. Diopsidic clinopyroxenes were present in relative stable concentrations, usually 20 – 30% (Figure 8) while the augitic grains were more abundant in the upper 300 m of the core.

Orthopyroxenes were distinguished from clinopyroxenes solely based on their straight extinction. Two types of orthopyroxene were identified, enstatite and hypersthene. The differences between them are the pleochroism and hexagonal terminations exhibited by hypersthene. Enstatite grains were relatively large and had a very characteristic etched feature. Enstatite was very abundant between 300 and 550 mbsf (Figure 8).

The amphibole group was also present in the samples, primarily in the form of hornblende; however there were small amounts of tremolite and anthophyllite. There were two main types of hornblende, a pleochroic green/brown variety and a brown variety. They were easily identifiable by their extinction angle, birefringence and amphibole cleavage. These grains also had the tendency to be fairly weathered due to their lower resistance to most types of weathering (Polozek and Ehrmann, 1998). The pleochroic green/brown variety was more abundant in the upper 300 m and the brown variety became abundant at 200 and 250 mbsf (Figure 8).

Volcanic glass was also relatively abundant throughout the core, especially towards the top where the glass accounted for about 50% of the grains in sample 36.74 mbsf. Many of the glass grains identified had inclusions of heavy minerals. These inclusions came mainly in the form of pyroxenes and oxides and usually several within one grain of glass. The pyroxene inclusions were typically long and prismatic. The volcanic glass was brown in color with a very smooth surface texture and was isotropic. The grains also usually had spherical and/or stretched vesicles. Though the primary goal of this study was to analyze the heavy mineral fraction, the Norland optical adhesive used was first tested on the light fraction of the sample at 36.74 mbsf. Upon a quick microscope check, approximately 100% of the grains from that light fraction were volcanic glass. This made it quite obvious that this sample was heavily influenced from volcanic activity and it is discussed later.

Other minerals identified optically were angular to sub rounded garnet which was mainly clear and sometimes pink. Percentages of garnet remained relatively stable through the upper 650 m, with a peak just above 300 mbsf (Figure 8). Epidote was usually rounded and was more abundant in the upper 250 m of the core, though there are some depths that did not have any epidote within that interval (Figure 8). Prismatic sillimanite was more abundant below 300 mbsf.

3.2 SEM/EDS Results

In contrast to the grain counting results, the EDS data shows a dominant presence of augite over diopside. This conclusion was drawn due to the presence of a small amount of iron in many of the clinopyroxene grains, which is not found in diopside. There were also spectra that represented pigeonite and titanaugite. Pigeonite was identified based on its calcium-poor, pyroxene chemistry. The hexagonal terminations and presence of titanium aided in the identification of titanaugite (Figure 9).

There were several types of amphiboles identified. The two main types were hornblende and kaersutite. Kaersutite (Figure 10) was more abundant in the upper 100 m of the core and hornblende was dominant below 100 m. Other amphiboles present in smaller amounts were gedrite and actinolite.

SEM/EDS analysis of garnet grains showed the presence of pyrope and almandine members, however it was common to see a combination of pyrope/spessartine members in one grain. The pyrope/spessartine grains had small peaks of Mn and were generally depleted in Mg and enriched in Fe (Figure 11).

A calcium magnesium carbonate was also found, identified as dolomite, exceptionally abundant at 599.02 mbsf (Figure 12). Some of those grains also contained a small amount of iron. There was also a significant amount of calcite identified at 250.54 mbsf (Figure 13).

Other minerals identified in smaller quantities were ilmenite (Figure 14), pyrite, and titanite/sphene (Figure 15). Pyrite was identified mainly between 250 and 350 mbsf and was relatively abundant. It was present as an alteration on minerals and as a cement.

Chromite and iron bearing minerals resembling ilmenite were found in the upper part of the core, specifically in the sample 28.22 mbsf. Rock fragments were also present throughout most of the core (Figure 16). Kaersutite was very abundant as a mineral within rock fragments. These rock fragments typically contained kaersutite. Volcanic glass was also identified (Figure 17), especially abundant 36.74 mbsf.

4. DISCUSSION

4.1 Mineral Source Regions

Table 3 was compiled based on the source rock regions of SMS and was derived from a number of published sources describing the mineralogy and petrology of surrounding rocks. The TAM and MVG are the primary source areas of SMS and changes in sediment input from these sources can help determine ice flow characteristics. They are very different from each other in terms of petrology and therefore can be easily distinguished. The TAM are composed of several metamorphic and sedimentary groups, intrusive and extrusive igneous, and basement rocks. The MVG is composed of alkali and basaltic volcanic rocks. There are minerals that are common to more than one group of rocks and an attempt was made to classify the minerals into the following rock groups: The Koettlitz Group (KG), Granite Harbour Intrusive Complex (GHIC), Beacon Supergroup (BSG), Ferrar Group (FG), and the McMurdo Volcanic Group (MVG).

4.2 Possible Sources of Heavy Minerals in the Upper ~650 m of AND-2A

Weight percentage of the heavy minerals is low compared to most tills in the TAM (Passchier, 2001), and there does not appear to be any correlation between any single mineral and weight percent of heavy minerals. A low weight percentage can indicate chemical weathering or erosion from a sedimentary or extrusive igneous source. Hoffman et al. (2010a) have described a low chemical index of alteration for the AND-2A core which suggests chemical weathering was not an influence on the sediment.

Based on the heavy mineral analysis, pyroxene is the most widespread group of heavy minerals in the McMurdo Sound region and the AND-2A core, and though they are the most abundant, they have proven useful because of their distinct source rocks. Diopsidic and green augitic clinopyroxenes in the core primarily had visible cleavage and are found throughout the TAM. In contrast, titanaugites and brown augite with generally poor or no visible cleavage are very diagnostic of the McMurdo volcanic group. The orthopyroxene enstatite is a known constituent of the Ferrar Group (Young and Ryburn, 1968; Damiani and Giorgetti, 2008) and the Ferrar Group can also be assumed as the source of hypersthene.

The green amphiboles in AND-2A, which are primarily Mg-hornblendes, and colorless amphiboles (anthophyllite and tremolite) are common rock forming minerals of many intermediate magmatic and metamorphic rocks. The probable sources for amphiboles in sediment cores of McMurdo Sound have been identified and described as the amphibolites of the Koettlitz Group (Polozek and Ehrmann, 1998; Polozek, 2000) and the granitoids of the Granite Harbour Intrusive Complex (Ghent and Henderson, 1968; Skinner and Ricker, 1968; Smillie, 1992). Brown hornblendes, identified as kaersutite via SEM/EDS, are common constituents of alkaline volcanic rocks such as trachybasalt, trachyandesites, and hornblende trachytes which have been described in the McMurdo Volcanic Group (LeMasurier and Thomson, 1990). This makes brown hornblende a clear indicator of glacial erosion from the MVG. Kaersutite was more abundant during SEM/EDS analysis than during grain counting. Since altered minerals can be primarily traced to the MVG, kaersutite can possibly be a significant component of them.

Many of the epidote group minerals identified show signs of recycling in the way of alteration and growth on the minerals and subrounded to rounded edges. These epidotes (such as clinozoisite) are very diagnostic of a sedimentary source such as the Beacon Supergroup or metasediments of the Koettlitz Group (Damiani and Giorgetti, 2008; La Prade, 1982).

Garnet is also a common mineral within the metasediments and orthogneisses of the Koettlitz Group and the Beacon Supergroup (Barrett, 1966; La Prade, 1982). Passchier (2001) has identified almandine garnet, pink in color, with a source of the Beacon Supergroup. Pink garnet was present in small amounts in the AND-2A core. A source for the pyrope and pyrope/spessartine members may be the Koettlitz Group.

Sillimanite and staurolite are metamorphic minerals and therefore are easily restricted to the TAM. Zircon has been identified in the Beacon Supergroup and Granite Harbour Intrusive Complex (La Prade, 1982; Ehrmann and Polozek, 1999), and tourmaline has been identified in the Beacon Supergroup (La Prade, 1982). Rutile is an accessory mineral characteristic of metamorphic rocks and a probable source would be the Koettlitz Group.

Titanite/sphene is an accessory mineral in the plutonic rocks and pegmatites of the Granite Harbour Intrusive Complex that was only identified via SEM. This is also a probable source for biotite (Ghent and Henderson, 1968; Skinner and Ricker, 1968; Smillie, 2000). Biotite has also been identified as an accessory mineral in the Beacon Supergroup (La Prade, 1982) and part of the Koettlitz Group (Stump, 1995).

Oxidized/altered minerals appear to be primarily coming from the MVG. By comparing oxidized down core distribution to that of apatite, epidote, and tourmaline, an opposite pattern can clearly be seen (Figure 18). Apatite, epidote, and tourmaline were chosen for comparison because of their restriction to the TAM and their similar down core distribution pattern. Oxidized grains also correlate well with abundances of volcanic glass. This suggests that the MVG is the most likely source for the oxidized minerals. Since oxidized minerals can be traced to the MVG and kaersutite was more abundant during SEM/EDS analysis than petrographic analysis, it can be assumed that a significant component of the oxidized minerals is kaersutite.

Opaque minerals can come from a variety of rock types and are present in all rocks around SMS, but a high concentration of them points to a volcanic source such as the MVG (Wimmenauer, 1985). Opaque minerals have been identified via SEM/EDS as illmenite, pyrite, chromite, and titanomagnetite.

Apatite is a well known accessory mineral of the Granite Harbour Intrusive Complex (Ghent and Henderson, 1968; Skinner and Ricker, 1968; Smillie, 1992), the Beacon Supergroup, and the Ferrar Group (Polozek and Ehrmann, 1998), though there is evidence to support a minor amount of angular apatite grains coming from the McMurdo Volcanic Group (Kyle, 1990). Since apatite is an uncommon accessory to mafic rocks, it is assumed for this study that all apatite is coming from the TAM, but is difficult to pinpoint a restricted source.

Volcanic glass has a definite provenance of the MVG, however only the brown varieties are present in this study. White, clear, brown, and green altered and unaltered glass have all been identified in the SMS core (Panter et al., 2008 in press). Clast petrology performed by Panter et al. (2008 in press) indicate that altered glass is primarily brown and has altered to hematite and other opaque minerals. A potential reason for the brown glass to only be present in this study may be related to potential differences in density between the different varieties of volcanic glass grains.

Pyrite has very few localities throughout the SMS region, such as thin layers within the Koettlitz Group (Stump, 1995), and the pyrite in the core is likely a product of diagenesis. An initial analysis of diagenesis from the core shows that carbonate cementation, authigenic pyrite formation, and alteration of volcanic glass are all major diagenetic processes taking place (Fielding et al., 2008, in press). Several factors responsible for the diagenetic activity include a high geothermal gradient, presence of alkaline formation waters, and abundance of chemically reactive volcanic constituents throughout the core (Fielding et al., 2008, in press).

4.3 Downcore Provenance Distribution of the Upper ~650 m of AND-2A

The results of grain counts versus depth are plotted in Figure 19 in which the heavy minerals have been broken up into two main groups, TAM and MVG. These are the two main source regions for the AND-2A core. This data is displayed as a total percentage of counts. It is evident from the data, that the TAM and MVG have been providing a continuous, but not equal, sediment supply to the SMS core site.

The top of the core, 36.74 mbsf, has a very large amount of volcanic glass. Since this interval is young, the glass is still very well preserved. With glass comprising almost half of the total minerals counted for in that interval (Table 2), there must have been volcanic activity that directly deposited sediment into this area. The MVG is relatively young, only about 20 Ma to present, but it is difficult to pinpoint the exact source for this volcanic glass deposit. The interval above 200.00 mbsf shows more volcanic influence, aside from the dip in MVG input around 100.00 mbsf.

The interval of 200.00 – 650.00 mbsf is clearly dominated by (a) source(s) located in the TAM. These minerals comprise about 60% of the counts throughout this interval whereas the MVG makes up the other 40%. There is also very little variation in the percentage of mineral groups between 350.00 and 550.00 mbsf.

In the sample 599.02 mbsf, there is an abundant amount of dolomite that is not seen anywhere else in the core. There are several outcrops of limestone and marble throughout the TAM, however there is one area to the south between the Byrd and Nimrod Glaciers (Figure 4) that contains ample exposures of these rocks. It is possible that there was erosion of these rocks and the material was transported to the SMS site by way of calving glaciers or grounded ice. Some of the dolomite grains were rounded, suggesting that was just the way it was eroded, or that they were not transported by glaciers.

Figure 20 shows the TAM and MVG groups overlaid on a graph based on how far from the average count percentage the counts are at each depth. As stated earlier, the interval at 36.74 mbsf shows a large influx of volcanic glass, about 50% of the counts for that sample. Because of its overwhelming presence, it is not included in this figure as it would skew the trends making it difficult to identify any other intervals of change. As a result, only the samples below 36.74 mbsf were included in the figure to provide a better analysis. This figure was primarily created in an attempt to make interpretations and tease out any sediment influx pulses that can be seen from the MVG during the TAM dominant interval and perhaps give some insight into volcanic activity. A total of five distinct intervals can be seen in which there is a greater than average abundance of MVG minerals and a less than average abundance of TAM minerals. Starting from the bottom of the core, these intervals are numbered 1-5 at 650.00 - 499.00, 499.00 - 345.00, 345.00 - 245.00, 245.00 150.00, and 150.00 mbsf up to the top of the core. These intervals begin with a higher amount of TAM minerals and end with a higher amount of MVG minerals.

Trends of the MVG minerals also correlate fairly well with the magnetic susceptibility data recorded during on-ice investigation (Figure 21). This suggests that the bulk of the magnetic minerals must be coming from a source within the MVG and that magnetic susceptibility can be used as an indicator of MVG input.

In an attempt to further distinguish minerals within the TAM, Figure 22 shows most TAM minerals normalized and broken up into four different groups: low grade metamorphic rocks, high grade metamorphic rocks, Beacon Supergroup/Granite Harbour Intrusive Complex (BSG/GHIC), and the Ferrar Group (FG). There are some minerals that were common to multiple groups and an attempt was made to classify them into their most likely source based upon publications (Barrett, 1966; Lopatin, 1972; La Prade 1982; Stump, 1995; Polozek and Ehrmann, 1998; Ehrmann and Polozek, 1999; Passchier, 2001, Damiani and Giorgetti, 2008). In some cases minerals were common constituents of two groups and were included in both (clinozoisite, epidote, hornblende). Some minerals were not included in the distinction because they were not unique to the area (non MVG clinopyroxenes, olivine, and others). In order to narrow the source of minerals common to multiple groups, the minerals were placed into each possible group to see if the distribution pattern of that group would change or remain the same. If the distribution pattern remained unchanged, the mineral would remain in that group. The Beacon

Supergroup and Granite Harbour Intrusive Complex were combined into one group because of their similar assemblages of heavy minerals.

Low grade metamorphic minerals were identified as andalusite, chlorite, clinozoisite, epidote, serpentine, and tourmaline. Minerals placed within the high grade metamorphic group were anthophyllite, pleochroic green/brown hornblende, kyanite, monazite, sillimanite, and staurolite. FG minerals consisted of enstatite and hypersthene. The BSG/GHIC consisted of biotite, chlorite, clinozoisite, epidote, garnet, pleochroic green/brown hornblende, tourmaline, and tremolite.

The FG, BSG/GHIC, and high grade metamorphic minerals remain relatively constant below 300 mbsf and the high grade metamorphic rocks and BSG/GHIC become more abundant above 200 mbsf. These three groups likely have a similar source for the interval 300 – 650 mbsf. Perhaps in the immediate location of the Koettlitz and Ferrar Glaciers is the most likely source. The rocks in this region are very diverse and could provide minerals representative of all the groups. The low grade metamorphic rocks remain a fairly constant low percentage through the core and are not discussed in further detail.

In the upper 200 m there are more minerals from the BSG/GHIC and high grade rocks present, such as pleochroic green/brown hornblende, tourmaline, epidote, biotite, and others. This also coincides with a general increase in deposition from the MVG at 200 m and above 50 m. It is likely that these sediments are coming from further south, such as the Beardmore, Shackelton, and/or Nimrod Glacier areas. Examples of rocks supplying the heavy minerals from this area would be the Nimrod Group, which has large sillimanite crystals (Passchier, 2001), and Beacon Supergroup exposures (Barrett, 1966).

There are some relatively large crystals of sillimanite in the AND-2A, but smaller and broken grains are also present.

4.4 Middle Miocene Glacial History

For the interval 300 – 650 mbsf, which covers a span of time from ~15 – 17 Ma, it is likely that there was a much less expansive ice sheet in which the ice grounding line was far from the SMS site. In this setting the WAIS may have been in decline, located somewhere in the southeastern Ross Sea, and of little or no influence to the core site. This conclusion can be made based on the low abundance of MVG minerals and high TAM minerals. The low presence of MVG heavy minerals suggests that there is no ice sheet present to directly erode these rocks. The primary form of terrigenous sedimentation likely came from calving glaciers of the Koettlitz Group and possibly windblown sediment. For this interval of the core, the heavy mineral assemblage remained relatively stable, especially 350 – 550 mbsf. During this interval input from the TAM is more abundant than the MVG (Figure 19), which suggests the WAIS was not proximal to the SMS site.

The upper 240 m of the core represents an environment in which the SMS core site was either covered in ice or the ice grounding line was in close proximity to the site. Under this scenario, sedimentary material was coming from as far south as the Beardmore Glacier and was being forced northward along the margin of the TAM by a large and dominant WAIS, as seen by the increase in BSG/GHIC and high grade metamorphic minerals (Figure 22) during this interval. This ice would then override the MVG and deposit sediment from both source regions, explaining the increase in MVG heavy minerals at 200 mbsf and above 50 mbsf. Licht et al. (2005) described a similar scenario for the last glacial maximum (Figure 23) and it can be used to describe the events observed in the AND-2A core. This supports the possible hiatuses seen in the upper 300 m of the core as an expanding, grounded ice sheet would remove any unconsolidated sediment and transport it away from the SMS site, creating the unconformities seen.

At 94.00 mbsf, there is a large drop in the quantity of MVG minerals (Figure 19). For this interval, the ice sheet may have retreated just south of Mt. Morning and Minna Bluff (Figure 24), still bringing debris from further south, but not eroding away much material from the MVG.

The interval between 240 and 300 mbsf is where a change in provenance takes place and an increase in high grade and BSG/GHIC minerals can be seen. This interval has an age range of approximately 13.8 - 15.4 Ma which is within the accepted ages of the MMCT cooling period (Shevenell, 2004). This supports the scenario mentioned in which there is a large expanding WAIS. The WAIS is more susceptible to environmental change, so a change in climate and ocean temperature would have a vast effect on the size of the ice sheet.

4.5 Comparison to SMS Team Findings

In the Initial Reports Volume of the SMS project, Panter et al. (2008, in press) analyzed a total of 103,696 clasts from the core. Provenance of the clasts was determined by logging descriptions and petrographic microscope analysis of the clasts. It was based on mineralogy and fabric and their two source areas were narrowed down to the Koettlitz

Glacier - Ferrar Glacier area and the Skelton Glacier - Darwin Glacier area. The former includes exposures of amphibolite grade metamorphic rocks and the Ferrar dolerites and the latter has exposures of greenschist grade metamorphic rocks. They interpreted an extensive ice sheet/shelf when a clast assemblage of the Skelton – Darwin Glacier was abundant.

Sandroni et al. (2010) give glacial interpretation based on provenance of clasts of boulder to granule in size, furthering the interpretations of Panter et al. (2008, in press). They present three alternating provenance phases. The first phase was for the lower part (775 - 626 mbsf) of the core, from which this heavy mineral study only has one sample . They find that this interval is dominated by Skelton Glacier input and is influenced by a large Antarctic ice sheet (Figure 25 A). Phase two is the interval 626 – 225 mbsf, in which there is a dominant input from the Koettlitz Glacier and then a change to Koettlitz – Skelton mixed at ~295 mbsf. They interpret this to be an interglacial setting (Figure 25 E,D). Phase three is for the interval 225 – 127 mbsf was interpreted to be glacial/interglacial fluctuations of Blue – Koettlitz Glacier region (Figure 25 C,D).

Wholerock geochemical analysis performed by Hoffman et al. (2010) shows a correlation with the heavy mineral analysis. They show a dominant provenance of MVG for the upper 200 m of the core and a TAM provenance for ~200 to 650 mbsf, however they make no interpretations about glacial conditions.

Passchier et al. (2009), have identified stacking patterns of facies associations in the AND-2A core and have classified them into two different motifs. These motifs correlate well with the interpretations of the heavy mineral data. Motif 1 represented a glacially dominated depositional environment and motif 2 represented an environment with a very dynamic ice sheet and open marine to iceberg deposition. Their study identified motif 1 from ~240 mbsf to the top of the core and motif 2 for the interval ~650 to 240 mbsf.

It is difficult to support the views presented by Panter et al. (2008, in press) and Sandroni et al. (2010) with a heavy mineral analysis of the fine sand fraction. Heavy minerals of the Skelton Glacier and Koettlitz Glacier areas are similar (biotite, amphiboles, clinopyroxene (Stump, 1995), except the addition of some higher metamorphic grade minerals in the Koettlitz Group (e.g. garnet). There are also some small outcrops of the Koettlitz Group within the area that feeds the Skelton Glacier (Stump, 1995). Therefore, a distinction between these two source areas is not possible from a heavy mineral standpoint. It is also difficult to make an interpretation based on the mineral percentages that are unique to the Koettlitz Group because there could be other sources further south. Panter et al. (2008, in press) and Sandroni et al. (2010) allude to the possibility of material coming from further south, but they do not discuss it in further detail.

There are known outcrops of high grade metamorphic rocks and sedimentary rocks further south of the Skelton Glacier, such as the Beardmore Glacier area (Barret and Elliot, 1972) or Shackelton Glacier area (Barret, 1966; La Prade, 1982). If outlet glaciers from the TAM were being forced northward by the WAIS, then there should also be evidence to support a provenance from these glaciers further south. The heavy mineral data supports the idea of sediment input from glaciers further south because of the increase in minerals such as hornblende, tourmaline, and epidote group in the upper portion of the core under the glacial condition described in the previous section.

It is possible that the heavy minerals of the fine sand fraction and the clasts are coming from different sources. If such is the case, then interpretations would be biased and based on the limitations of the size fraction researched. Similarly, the wholerock geochemistry may not be representative of the chemistry of the heavy mineral fraction because the 630 – 250 μm heavy minerals only accounts for 1 – 3% of the weight percentage.

Collectively, all of the work performed by the team members, including this heavy mineral analysis, suggests that there is a period between 300 and 650 mbsf (15 – 17 Ma) in which the ice sheet is not proximal to the SMS core site and that there is deposition from TAM derived sediment from the Koettlitz Glacier area. Between 240 and 300 mbsf a change took place in both sediment provenance and glacial setting. This change implies an expanded ice sheet for the upper 240 m of the core that brought sediment derived from glaciers further south as well as the erosion of the MVG.

5. CONCLUSION

The Southern McMurdo Sound region of Antarctica is an ideal place to study sediment history because of the half graben structure formed during rifting of the WAIS and uplift of the Transantarctic Mountains. A nearly complete sediment record of the Early-Middle Miocene has now been recovered along the shelf of Antarctica for the first time. The area has experienced sediment deposition from several sources during the past 17 Myr, including suites of rocks located in the TAM and volcanic rocks of the MVG.

Using heavy liquid separation techniques, heavy minerals separates were created for the fine sand fraction (63 – 250 μm) from 24 samples throughout the upper 650 m of the AND-2A core. From these separates grains mounts were created and identified (300 grains per slide) using a petrographic microscope as well as identification of some samples in an SEM/EDS.

Using the count and EDS data, the heavy minerals were separated into the diagnostic groups of TAM and MVG. This has proved very useful in the determination of sediment provenance. Furthermore, separation of the TAM minerals into separate groups has given insight into possible glacial conditions during the past 17 Myr. The heavy mineral data from this core has shown several variations in ice flow patterns and evidence to support ice growth during the MMCT.

The interval 300 – 650 m (15 – 17 Ma) appears to be relatively stable in terms of heavy mineral deposition in the SMS region. This part of the core offers a high resolution and minimal hiatuses caused by expansion of ice sheets. Mineral concentrations remain relatively constant with a primary source of the Koettlitz Glacier in the TAM. This suggests a period of time in which the ice sheets may have been smaller and glacial grounding lines were far south of the SMS core site. The WAIS would not have played a major role in sediment deposition at the SMS site during this time.

The heavy mineral data from the upper 240 m of the core represents a period of ice sheet expansion in which the grounding line is either at or north of the SMS core site. Under this scenario, a larger and dominant WAIS would have existed, causing drainage patterns from glaciers in the south to flow in a more northerly direction along the margin of the TAM. This explains increased percentages of BSG, and higher grade metamorphic mineral deposition in the upper portion of the core and increased deposition of the MVG at 200 and above 50 mbsf. There is a decrease in MVG at ~100 mbsf while concentrations of BSG/GHIC and high grade metamorphic rocks still increase. At this depth, the ice sheet may have retreated just south of Mt. Morning and Minna Bluff of the MVG, still depositing material from further south by calving glaciers, but not directly eroding the MVG.

The interval 240 – 300 mbsf is the point at which a change in heavy mineral provenance can be seen. The age of this interval (13.8 – 15.4 Ma) correlates well to the age of the MMCT. This was a gradual cooling period in Earth's history and supports the idea of the expansion of ice represented by the heavy mineral data.

REFERENCES

Acton, G., Florindo, F., Jovane, L., Lum, B, Ohneiser, C., Sagnotti, L., Strade, E., Verosub, K.L., Wilson, G.S., & ANDRILL-SMS Science Team, 2008 In Press. *Palaeomagnetism of the AND-2A core, ANDRILL Southern McMurdo Sound Project, Antarctica.* Terra Antarctica, vol. 15(1), p. 193-210.

Anderson, J.B., 1999. *Antarctic marine geology.* Cambridge University Press, p 1-57

ANDRILL SMS Science Team, 2010. *An integrated age model for the ANDRILL-2A Core.* In Kontar, K., Harwood, D.M., Florindo, F., and Fischbein, S. (eds), 2010. *ANDRILL Southern McMurdo Sound Project, Science Integration Workshop – Program and Abstracts.* ANDRILL Contribution #16, ANDRILL Science Management Office, Univ. of Nebraska, Lincoln, NE, pp. 113.

Barret, P.J., 1966. *Petrology of some beacon rocks between the Axel Heiberg and Shackelton Glaciers, Queen Maud Range, Antarctica.* Journal of Sedimentary Petrology, Vol. 36, No. 3, p. 794-805.

Barret, P. J., Elliot, D.H., 1972. *The Early Mesozoic volcaniclastic Prebble Formation, Beardmore Glacier Area,* in Adie R.J., ed., Antarctic Geology and Geophysics; Oslo, Universitetsforlaget, p. 403-409.

Barret, P. J., 1991. *The Devonian to Triassic Beacon Supergroup of the Transantarctic Mountains and correlatives in other parts of Antarctica.* In: Tingey, R. J. ed. The Geology of Antarctica. Oxford Monographs on Geology and Geophysics. Oxford, Clarendon Press, p. 120-152.

Black, L.P., James, P.R., Harley, S.L., 1983. *Geochronology and geological evolution of metamorphic rocks in the Field Islands area, East Antarctica.* Journal of Metamorphic Geology, vol. 1, p 277-303.

Borg, S.G., Goodge, J.W., Bennett, V.C., DePaolo, D.J., 1987. *Geochemistry of granites and metamorphic rocks: central Transantarctic Mountains.* Ant. J. U.S., vol. 22, p 21-23.

Damiani, D., Giorgetti, G., 2008. *Provenance of glacial-marine sediments under the McMurdo/Ross Ice Shelf (Windless Bight, Antarctica): Heavy minerals and geochemical data.* Paleogeography, Paleoclimatology, Paleoecology, v. 260, p. 262-283.

DeConto, R. M. and Pollard, D., 2003, *Rapid Cenozoic glaciation of Antarctica induced by declining atmospheric CO2.* Nature, vol. 421, p. 245-249.

Del Carlo, P., Panter, K.S., Bassett, K., Bracciali, L., Di Vincenzo, G., Rocchi, S., 2009. *The Upper lithostratigraphic unit of the ANDRILL AND-2A Core (Southern McMurdo Sound Antarctica): Local Pleistocene volcanic sources, paleoenvironmental implications and subsidence in the southern Victoria Land Basin.* Global and Planetary Change, vol. 69, p. 142-161.

Denton, V.H., Hughes, T.J., 1981. *The Arctic Ice Sheet: An outrageous hypothesis.* In G.H. Denton and T.J. Hughes, eds., The Last Great Ice Sheets. John Wiley & Sons, New York, p. 437-467.

Elliot D. H., 1975. *Tectonics of Antarctica: a review.* American Journal of Science, v. 275, p. 45-106.

Ehrmann, W., Polozek, K., 1999. *The heavy mineral record in the Pliocene to Quaternary sediments of the CIROS-2 drill core, McMurdo Sound, Antarctica.* Sedimentary Geology, v. 128, p. 223-244.

Fielding, C.R., Atkins, C.B., Bassett, K.N., Browne, G.H., Dunbar, G.B., Field, B.D., Frank, T.D., Krissek, L.A., Panter, K.S., Passchier, S., Pekar, S.F., Sandroni, S., Talarico, F., & the ANDRILL-SMS Science Team, 2008 in press. *sedimentology and stratigraphy of the AND-2A Core, ANDRILL Southern McMurdo Sound Project, Antarctica.* Terra Antarctica, vol. 15(1), p. 77-112.

Fitzgerald, P., 2002. *Tectonics and landscape evolution of the Antarctic plate since the breakup of Gondwana, with an emphasis on the West Antarctic Rift System and the Transantarctic Mountains.* Royal Society of New Zealand Bulletin, v. 35, p. 453-469.

Ghent E.D., Henderson, R.A., 1968. *Geology of the Mt Falconer Pluton, lower Taylor Valley, Sourth Victoria Land, Antarctica.* New Zealand Journal of Geology and Geophysics, v. 11, p. 851-879.

Harwood, D.M., Florindo, F., Levy, R.H., Fielding, C.R., Pekar, S.F., Speece, M. and SMS Science Team., 2006. *ANDRILL Southern McMurdo Sound Project Scientific Prospectus.* ANDRILL Contribution 5.

Hoffman, S., von Eynatten, H., Kuhn, G., 2010a. *Chemical weathering of Miocene sediments from the ANDRILL AND-2A core, Ross Sea, Antarctica* In Kontar, K., Harwood, D.M., Florindo, F., and Fischbein, S. (eds), 2010. *ANDRILL Southern McMurdo Sound Project, Science Integration Workshop – Program and Abstracts.* ANDRILL Contribution #16, ANDRILL Science Management Office, Univ. of Nebraska, Lincoln, NE, pp. 113.

Hoffman, S., von Eynatten, H., Kuhn, G., 2010b. *Geochemical record of Miocene sediment provenance in the McMurdo Sound, ANDRILL AND-2A, Ross Sea,* *Antarctica.* In Kontar, K., Harwood, D.M., Florindo, F., and Fischbein, S. (eds), 2010. *ANDRILL Southern McMurdo Sound Project, Science Integration Workshop – Program and Abstracts.* ANDRILL Contribution #16, ANDRILL Science Management Office, Univ. of Nebraska, Lincoln, NE, pp. 113.

Kontar, K., Harwood, D.M., Florindo, F., and Fischbein, S. (eds), 2010. *ANDRILL Southern McMurdo Sound Project, Science Integration Workshop – Program and Abstracts.* ANDRILL Contribution #16, ANDRILL Science Management Office, Univ. of Nebraska, Lincoln, NE, pp. 113.

Kyle, P.R., 1990. *McMurdo Volcanic Group, Western Ross Embayment.* In: LeMasurier, W.E., Thomson, J.W. (Eds.), Volcanoes of the Antarctic Plate and Southern Oceans. Antarctic Research, v 48, p. 81-123.

La Prade, K.E., 1982. *Petrology and petrography of the Beacon Supergroup, Shackleton Glacier area, Queen Maud Range, Transantarctic Mountains, Antarctica.* In: Craddock, C. (Ed.), Antarctic Geoscience. Univ. of Wisconsin Press, Madison, p. 581–590

LeMasurier, W. E., Thomson, J.W., 1990. *Volcanoes of the Antarctic plate and Southern Oceans.* Antarctic Research Series v. 48. Washington D.C., American Geophysical Union.

Lewis, A.R., Marchant, D.R., Ashworth, A.C., Hemming, S.R., Machlus, M.L., 2007. *Major middle Miocene global climate change: Evidence from East Antarctica and the Transantarctic Mountains.* Geological Society of America Bulletin, v. 119, p. 1449-1461.

Licht, K.J., Lederer, J.R., Swope, J., 2005. *Provenance of LGM glacial till (sand fraction) across the Ross Embayment, Antarctica.* Quaternary Science Reviews, vol. 24, p. 1499-1520.

Lopatin, B.G., 1972. *Basement complex of the McMurdo Oasis, southern Victoria Land.* In: R.J. Adie, Editor, Antarctic Geology and Geophysics, IUGS Series B vol. 1, p. 287–292

Mange, M.A., Maurer, H.F.W., 1992. *Heavy minerals in colour*. Chapman and Hall, London, 147 pp

Naish T., Powell R., & Levy, R. (Eds.), 2007. *Studies from the ANDRILL, McMurdo Ice Shelf Project, Antarctica, Initial Science Report on AND-1B.* Terra Antarctica, vol. 14(3), p. 121- 327.

Panter, K.S., Talarico, F.M., Bassett, K., Del Carlo, P., Field, B., Frank, T., Hoffmann, S., Kuhn, G., Reichelt, L., Sandroni, S., Taviani, M., Bracciali, L., Cornamusini, G., von Eynatten, H., Rocchi, S., & the ANDRILL-SMS Science Team, 2008 in press. *Petrologic and Geochemical Composition of the AND-2A Core, ANDRILL Southern McMurdo Sound Project, Antarctica.* Terra Antarctica, vol. 15(1), p. 147-192.

Passchier, S., 2001. *Provenance of the Sirius Group and related Upper Cenozoic glacial deposits from the Transantarctic Mountains, Antarctica: Relation to landscape evolution and ice-sheet drainage.* Sedimentary Geology, v. 144, p. 263-290.

Passchier, S., 2007. *The use of heavy minerals in the reconstruction of ice-sheet drainage patterns: An example from the edge of the East Antarctic Ice Sheet.* Developments in Sedimentology, vol. 58, 677-699.

Passchier, S., Falk, C., Fielding, C.R., Florindo, F., Harwood, D.M., Pekar, S.F., 2009. *Controls on glacial facies distribution in the AND-2A Core, Antarctica, across the Middle Miocene Transition.* Eos trans. AGU, v. 90(52), Fall meet. Suppl., Abstract C23A-0493.

Pollard, D., DeConto, R.M., 2009. *Modeling West Antarctic ice sheet growth and collapse through the past five million years.* Nature, v. 458, p. 329-332.

Polozek, K., 2000. *Distribution of heavy minerals in CRP-2/2A, Victoria land Basin, Antarctica.* Terra Antarctica, v. 7, p. 567-573.

Polozek, K., Ehrmann, W., 1998. *Distribution of heavy minerals in CRP-1.* Terra Antarctica, v. 5(3), p. 633-638.

Reed, S.J.B., 2005. *Electron microprobe analysis and scanning electron microscopy in geology.* 2nd ed., Cambridge University Press, New York.

Sandroni, S., Talarico, F.M., 2006. *Analysis of clast lithologies from CIROS-2 core, New Harbour, Antarctica — Implications for ice flow directions during Plio-Pleistocene time.* Palaeogeography, Palaeoclimatology, Palaeoecology, 231, p. 215– 232

Shevenell, A.E., Kennett, J.P., Lea, D.W., 2004. *Middle Miocene Southern Ocean cooling and Antarctic cryosphere expansion.* Science, v. 305, p. 1766-1770.

Skinner, D.N.B., Ricker, J., 1968. *The geology of the region between the Mawson and Priestley Glaciers, North Victoria Land, Antarctica, Part 1 – Basement meta-sedimentary and igneous rocks.* New Zealand Journal of Geology and Geophysics, v. 11, p. 1009-1075.

Smillie, R.W., 1992. *Suite subdivision and petrological evolution of granitoids from the Taylor Valley and Ferrar Glacier Region, Sourth Victoria Land.* Antarctic Science, v. 4, p. 71-87.

Stump, E., 1995. *The Ross Orogen of the Transantarctic Mountains.* Cambridge University Press, New York.

Talarico, F.M., Zattin, M., Sandroni, S., 2010. *Integrated provenance and detrital thermochronology in the ANDRILL AND-2A drill core: first evidence of Late Oligocene to Early Miocene exhumation of the Transantarctic Mountains.* In Kontar, K., Harwood, D.M., Florindo, F., and Fischbein, S. (eds), 2010. *ANDRILL Southern McMurdo Sound Project, Science Integration Workshop – Program and Abstracts.* ANDRILL Contribution #16, ANDRILL Science Management Office, Univ. of Nebraska, Lincoln, NE, pp. 113.

Wimmenauer, W., 1985. *Petrographie der magmatischen und metamorphen Gesteine.* Enke, Stuttgart, p. 382.

Young, D.J., Ryburn, R.J., 1968. *The geology of Buckley and Darwin Nunataks, Beardmore Glacier, Ross Dependency, Antarctica.* New Zealand Journal of Geology and Geophysics, v. 11(4), p. 922-939.

Zachos, J.C., Dickens, G.R., Zeebe, R.E., 2008. *An Early Cenozoic perspective on greenhouse warming and carbon-cycle dynamics.* Nature, vol. 451, p. 279-283.

Appendix

Depth (mbsf)	22.14	36.74	48.27	94.00	126.98	152.01	201.01	240.80	250.54	286.01	295.04	308.01	319.96	351.02	393.00	423.96	446.38	469.48	503.00	551.99	559.00	599.02	649.10
Andalusite	1	0	0	0	0	0	0	0	0	0	0	0	0	0	0	0	0	0	0	0	0	0	0
Anthophyllite	3	0	0	0	9	6	0	0	4	1	4	4	3	1	0	1	0	6	0	0	1	0	0
Apatite	4	1	0	10	3	5	0	10	2	9	11	6	1	0	6	5	5	9	8	3	3	10	10
Augite, brown	37	4	6	5	6	24	0	0	3	0	0	1	3	0	0	0	0	0	0	0	39	4	0
Augite, green	7	7	9	27	9	8	18	2	11	11	10	14	4	1	0	3	0	3	1	2	17	1	0
Augite, green/brown	8	0	29	0	0	0	0	0	0	0	0	0	0	0	0	22	15	0	0	0	0	0	0
Augite, purple	0	3	0	0	3	0	5	0	4	1	5	7	5	0	4	10	0	0	0	3	1	3	0
Augite, red/pink	17	14	45	8	14	9	5	8	11	6	13	0	10	2	16	11	9	13	5	10	20	6	0
Biotite	0	0	11	0	3	0	0	0	0	2	0	1	0	0	0	3	0	0	0	0	1	0	0
Calcite	0	0	0	0	0	0	0	0	41	0	0	0	0	0	0	0	0	0	0	0	0	0	0
Cassiterite	0	0	0	0	0	0	0	0	1	0	0	0	0	0	0	0	0	0	0	0	0	0	0
Chlorite	0	0	0	0	0	0	0	0	0	0	0	0	0	0	0	0	0	0	0	1	0	0	0
Clinozoisite	0	0	22	0	0	1	0	24	13	8	0	0	0	0	8	0	0	0	8	0	0	0	0
Colorless clinopyroxene	0	0	0	0	0	0	0	0	0	0	0	0	0	0	0	0	0	27	0	0	0	0	0
Dark Red unknown	0	6	0	0	0	0	0	0	0	0	0	0	0	0	0	0	0	0	0	0	0	0	0
Dillage	0	0	1	0	0	0	1	0	0	0	0	0	0	0	0	0	0	0	0	0	0	0	0
Diopside	7	26	39	88	68	87	59	80	56	81	62	90	128	87	72	85	119	84	97	112	53	44	13
Dolomite	0	0	0	0	0	0	0	0	0	0	0	0	0	0	0	0	0	0	0	0	0	34	0
Enstatite	2	4	4	15	26	0	14	44	6	15	13	27	42	29	49	22	18	34	43	29	4	18	64
Epidote	1	0	0	0	5	0	0	0	0	0	1	0	0	3	5	0	0	2	0	0	0	0	18
Garnet	4	1	1	8	9	5	5	4	5	26	0	7	1	6	1	6	3	4	4	5	10	7	32
Glass w/inclusions	32	138	8	0	0	0	0	5	5	21	24	9	3	1	2	13	9	0	11	2	0	7	23
Hornblende br	0	0	0	0	0	0	8	0	6	4	1	0	0	0	0	2	0	0	0	0	3	0	0
Hornblende gr/br	8	14	19	27	27	17	15	14	15	14	9	8	19	8	15	12	0	16	0	4	6	5	0
Hypersthene	3	4	15	2	4	0	6	3	1	2	1	4	0	3	0	5	1	3	0	2	1	0	0
Kyanite	5	0	0	0	0	0	0	0	0	0	0	0	0	2	1	1	2	0	0	0	0	0	0
Monazite	0	0	0	11	2	2	0	0	5	0	0	0	0	0	0	0	0	1	0	0	0	0	0
Muscovite	0	2	0	0	0	0	0	0	0	0	0	0	0	0	0	0	0	0	0	0	0	0	0
Olivine	2	0	0	0	0	0	1	0	0	0	0	0	0	0	0	0	0	0	0	0	0	0	0
Opaque	25	7	12	3	7	0	0	2	5	3	4	9	0	24	1	4	2	1	0	0	8	0	12
Oxidized/Altered	110	46	39	66	87	88	151	61	80	89	110	97	76	134	83	93	92	88	117	108	127	57	97
Rock fragment	0	0	0	7	3	3	4	5	0	2	6	11	0	0	0	3	0	1	0	6	5	3	0
Rutile	1	0	0	0	2	0	0	0	0	0	2	0	0	0	0	0	0	1	0	0	0	0	0
Serpentine	0	0	0	0	1	0	0	0	0	0	0	0	0	0	0	0	0	0	0	0	0	0	0
Sillimanite	0	0	1	0	11	4	2	5	6	0	2	4	13	0	13	0	22	4	8	20	0	0	26
Sphene	0	0	3	0	1	0	0	0	0	0	0	0	0	0	0	0	0	1	0	0	1	0	0
Staurolite	0	0	4	0	0	0	0	0	0	0	0	0	0	0	1	0	0	0	0	0	0	0	0
Topaz	0	0	0	13	0	1	0	0	0	0	6	0	0	0	1	0	0	0	0	0	0	0	7
Tourmaline	9	12	26	2	8	3	0	2	2	3	6	3	3	1	11	0	0	3	7	0	0	2	0
Tremolite	0	0	0	0	0	24	0	0	0	0	0	0	0	0	0	0	0	0	0	0	0	0	0
Unknown	5	7	0	10	7	5	2	37	18	3	0	0	1	0	3	0	0	0	0	0	8	94	0
Unknown Amphib	0	0	0	0	0	0	0	0	0	0	4	0	1	0	0	0	0	0	0	0	0	0	0
Zircon	0	0	0	0	0	1	0	0	0	0	1	3	1	0	0	1	0	0	0	0	0	0	0
Total	291	296	294	302	315	293	296	306	300	301	295	305	314	302	292	302	297	301	309	307	308	295	302

Figure A1 – Comprehensive figure of all heavy mineral counts.

Figure A2. Comprehensive figure of all heavy mineral count percentages

Depth (mbsf)	22.14	36.74	48.27	94.00	126.98	152.01	201.01	240.81	250.52	286.00	295.04	308.01	319.96	351.02	391.00	403.96	446.32	469.48	503.00	551.99	559.00	599.02	649.10
Andalusite	0.34	0.00	0.00	0.00	0.00	0.00	0.00	0.00	0.00	0.00	0.00	0.00	0.00	0.00	0.00	0.00	0.00	0.00	0.00	0.00	0.00	0.00	0.00
Anthophyllite	1.03	0.00	0.00	0.00	2.86	2.05	0.00	0.00	1.33	0.33	1.36	1.31	0.96	0.33	0.00	0.33	0.00	1.99	0.00	0.00	0.32	0.00	0.00
Apatite	1.37	0.34	0.00	3.31	0.95	1.71	0.00	3.27	0.67	2.99	3.73	1.97	0.32	0.00	2.05	1.66	1.68	2.99	2.59	0.98	0.97	3.39	3.31
Augite, brown	12.71	1.35	2.04	1.66	1.90	8.19	0.00	0.00	1.00	0.00	0.00	0.33	0.96	0.00	0.00	0.00	0.00	0.00	0.00	0.00	12.66	1.36	0.00
Augite, green	2.41	2.36	3.06	8.94	2.86	2.73	6.08	0.65	3.67	3.65	3.39	4.59	1.27	0.33	0.00	0.99	0.00	1.00	0.32	0.65	5.52	0.34	0.00
Augite, green/brown	2.75	0.00	9.86	0.00	0.00	0.00	0.00	0.00	0.00	0.00	0.00	0.00	0.00	0.00	0.00	7.28	5.05	0.00	0.00	0.00	0.00	0.00	0.00
Augite, red/purple	0.00	1.01	0.00	0.00	0.95	0.00	1.69	0.00	1.33	0.33	1.69	2.30	1.59	0.00	1.37	3.31	0.00	0.00	0.00	0.98	0.32	1.02	0.00
Augite, red/pink	5.84	4.73	15.31	2.65	4.44	3.07	1.69	2.61	3.67	1.99	4.41	0.00	3.18	0.66	5.48	3.64	3.03	4.32	1.62	3.26	6.49	2.03	0.00
Biotite	0.00	0.00	3.74	0.00	0.95	0.00	0.00	0.00	0.00	0.66	0.00	0.33	0.00	0.00	0.00	0.99	0.00	0.00	0.00	0.00	0.32	0.00	0.00
Cassiterite	0.00	0.00	0.00	0.00	0.00	0.00	0.00	0.00	0.33	0.00	0.00	0.00	0.00	0.00	0.00	0.00	0.00	0.00	0.00	0.00	0.00	0.00	0.00
Chlorite	0.00	0.00	0.00	0.00	0.00	0.00	0.00	0.00	0.00	0.00	0.00	0.00	0.00	0.00	0.00	0.00	0.00	0.00	0.00	0.33	0.00	0.00	0.00
Clinozoisite	0.00	0.00	7.48	0.00	0.00	0.34	0.00	7.84	4.33	2.66	0.00	0.00	0.00	0.00	2.74	0.00	0.00	0.00	2.59	0.00	0.00	0.00	0.00
Dark Red unknown	0.00	2.03	0.00	0.00	0.00	0.00	0.00	0.00	0.00	0.00	0.00	0.00	0.00	0.00	0.00	0.00	0.00	0.00	0.00	0.00	0.00	0.00	0.00
Dillage	0.00	0.00	0.34	0.00	0.00	0.00	0.34	0.00	0.00	0.00	0.00	0.00	0.00	0.00	0.00	0.00	0.00	0.00	0.00	0.00	0.00	0.00	0.00
Diopside	2.41	8.78	13.27	29.14	21.59	29.69	19.93	26.14	18.67	26.91	21.02	29.51	40.76	28.81	24.66	28.15	40.07	27.91	31.39	36.48	17.21	14.92	4.30
Dolomite	0.00	0.00	0.00	0.00	0.00	0.00	0.00	0.00	0.00	0.00	0.00	0.00	0.00	0.00	0.00	0.00	0.00	0.00	0.00	0.00	0.00	11.53	0.00
Enstatite	0.69	1.35	1.36	4.97	8.25	0.00	4.73	14.38	2.00	4.98	4.41	8.85	13.38	9.60	16.78	7.28	6.06	11.30	13.92	9.45	1.30	6.10	21.19
Epidote	0.34	0.00	0.00	0.00	1.59	0.00	0.00	0.00	0.00	0.00	0.34	0.00	0.00	0.99	1.71	0.00	0.00	0.66	0.00	0.00	0.00	0.00	5.96
Garnet	1.37	0.34	0.34	2.65	2.86	1.71	1.69	1.31	1.67	8.64	0.00	2.30	0.32	1.99	0.34	1.99	1.01	1.33	1.29	1.63	3.25	2.37	10.60
Glass w/inclusions	11.00	46.62	2.72	0.00	0.00	0.00	0.00	1.63	1.67	6.98	8.14	2.95	0.96	0.33	0.68	4.30	3.03	0.00	3.56	0.65	0.00	2.37	7.62
Hornblende br	0.00	0.00	0.00	0.00	0.00	0.00	2.70	0.00	2.00	1.33	0.34	0.00	0.00	0.00	0.00	0.66	0.00	0.00	0.00	0.00	0.97	0.00	0.00
Hornblende gr/br	2.75	4.73	6.46	8.94	8.57	5.80	5.07	4.58	5.00	4.65	3.05	2.62	6.05	2.65	5.14	3.97	0.00	5.32	0.00	1.30	1.95	1.69	0.00
Hypersthene	1.03	1.35	5.10	0.66	1.27	0.00	2.03	0.98	0.33	0.66	0.34	1.31	0.00	0.99	0.00	1.66	0.34	1.00	0.00	0.65	0.32	0.00	0.00
Kyanite	1.72	0.00	0.00	0.00	0.00	0.00	0.00	0.00	0.00	0.00	0.00	0.00	0.00	0.66	0.34	0.33	0.67	0.00	0.00	0.00	0.00	0.00	0.00
Monazite	0.00	0.00	0.00	3.64	0.63	0.68	0.00	0.00	1.67	0.00	0.00	0.00	0.00	0.00	0.00	0.00	0.00	0.33	0.00	0.00	0.00	0.00	0.00
Muscovite	0.00	0.68	0.00	0.00	0.00	0.00	0.00	0.00	0.00	0.00	0.00	0.00	0.00	0.00	0.00	0.00	0.00	0.00	0.00	0.00	0.00	0.00	0.00
Olivine	0.69	0.00	0.00	0.00	0.00	0.00	0.34	0.00	0.00	0.00	0.00	0.00	0.00	0.00	0.00	0.00	0.00	0.00	0.00	0.00	0.00	0.00	0.00
Opaque	8.59	2.36	4.08	0.99	2.22	0.00	0.00	0.65	1.67	1.00	1.36	2.95	0.00	7.95	0.34	1.32	0.67	0.33	0.00	0.00	2.60	0.00	3.97
Oxidized/Altered	37.80	15.54	13.27	21.85	27.62	30.03	51.01	19.93	26.67	29.57	37.29	31.80	24.20	44.37	28.42	30.79	30.98	29.24	37.86	35.18	41.23	19.32	32.12
Rutile	0.34	0.00	0.00	0.00	0.63	0.00	0.00	0.00	0.00	0.00	0.68	0.00	0.00	0.00	0.00	0.00	0.00	0.33	0.00	0.00	0.00	0.00	0.00
Serpentine	0.00	0.00	0.00	0.00	0.32	0.00	0.00	0.00	0.00	0.00	0.00	0.00	0.00	0.00	0.00	0.00	0.00	0.00	0.00	0.00	0.00	0.00	0.00
Sillimanite	0.00	0.00	0.34	0.00	3.49	1.37	0.68	1.63	2.00	0.00	0.68	1.31	4.14	0.00	4.45	0.00	7.41	1.33	2.59	6.51	0.00	0.00	8.61
Sphene	0.00	0.00	1.02	0.00	0.32	0.00	0.00	0.00	0.00	0.00	0.00	0.00	0.00	0.00	0.00	0.00	0.00	0.33	0.00	0.00	0.32	0.00	0.00
Staurolite	0.00	0.00	1.36	0.00	0.00	0.00	0.00	0.00	0.00	0.00	0.00	0.00	0.00	0.00	0.34	0.00	0.00	0.00	0.00	0.00	0.00	0.00	0.00
Topaz	0.00	0.00	0.00	4.30	0.00	0.34	0.00	0.00	0.00	0.00	2.03	0.00	0.00	0.00	0.34	0.00	0.00	0.00	0.00	0.00	0.00	0.00	2.32
Tourmaline	3.09	4.05	8.84	0.66	2.54	1.02	0.00	0.65	0.67	1.00	2.03	0.98	0.96	0.33	3.77	0.00	0.00	1.00	2.27	0.00	0.00	0.68	0.00
Tremolite	0.00	0.00	0.00	0.00	0.00	8.19	0.00	0.00	0.00	0.00	0.00	0.00	0.00	0.00	0.00	0.00	0.00	0.00	0.00	0.00	0.00	0.00	0.00
Unknown	1.72	2.36	0.00	3.31	2.22	1.71	0.68	12.09	6.00	1.00	0.00	0.00	0.32	0.00	1.03	0.00	0.00	0.00	0.00	0.00	2.60	31.86	0.00
Unknown clinopyroxene	0.00	0.00	0.00	0.00	0.00	0.00	0.00	0.00	0.00	0.00	0.00	0.00	0.00	0.00	0.00	0.00	0.00	8.97	0.00	0.00	0.00	0.00	0.00
Rock fragment	0.00	0.00	0.00	2.32	0.95	1.02	1.35	1.63	0.00	0.66	2.03	3.61	0.00	0.00	0.00	0.99	0.00	0.33	0.00	1.95	1.62	1.02	0.00
Unknown Amphibole	0.00	0.00	0.00	0.00	0.00	0.00	0.00	0.00	0.00	0.00	1.36	0.00	0.32	0.00	0.00	0.00	0.00	0.00	0.00	0.00	0.00	0.00	0.00
Zircon	0.00	0.00	0.00	0.00	0.00	0.34	0.00	0.00	0.00	0.00	0.34	0.98	0.32	0.00	0.00	0.33	0.00	0.00	0.00	0.00	0.00	0.00	0.00
Calcite	0.00	0.00	0.00	0.00	0.00	0.00	0.00	0.00	13.67	0.00	0.00	0.00	0.00	0.00	0.00	0.00	0.00	0.00	0.00	0.00	0.00	0.00	0.00
Total	100.00	100.00	100.00	#####	100.00	100.00	100.00	100.00	100.00	100.00	100.00	100.00	100.00	100.00	100.00	100.00	100.00	100.00	100.00	100.00	100.00	100.00	100.00

Figures

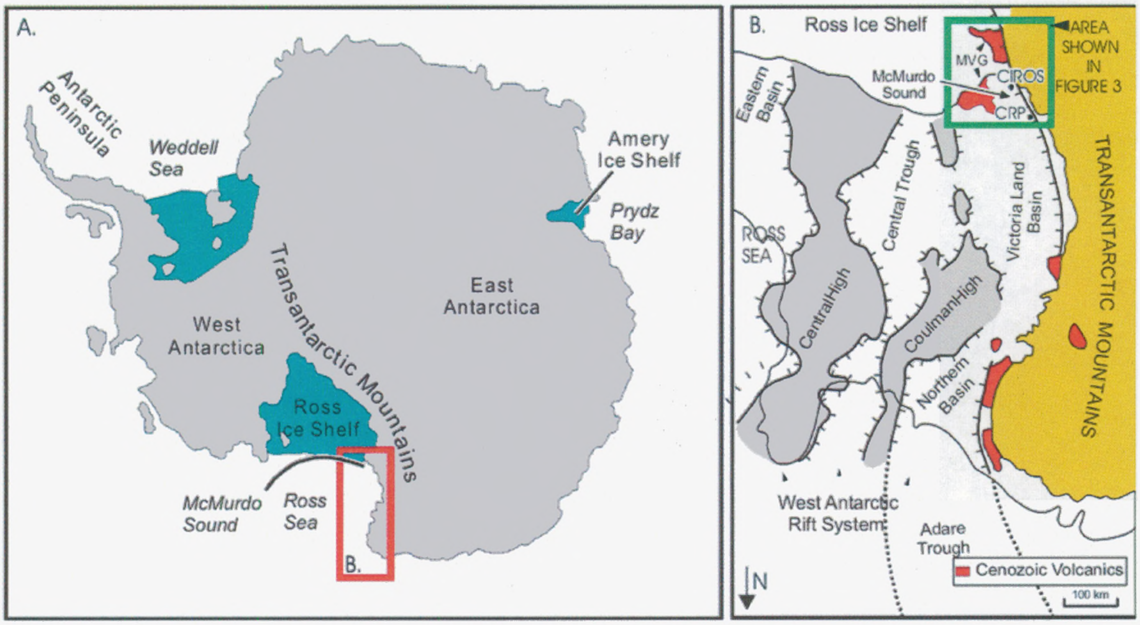
A.
Antarctic Peninsula
Weddell Sea
Amery Ice Shelf
Prydz Bay
East Antarctica
West Antarctica
Transantarctic Mountains
Ross Ice Shelf
McMurdo Sound
Ross Sea
B.
B.
Ross Ice Shelf
MVG
McMurdo Sound
CIROS
CRP
AREA SHOWN IN FIGURE 3
Eastern Basin
Central Trough
Victoria Land Basin
TRANSANTARCTIC MOUNTAINS
ROSS SEA
CentralHigh
CoulmanHigh
Northern Basin
West Antarctic Rift System
Adare Trough
Cenozoic Volcanics
100 km
N

Figure 1 – (a) Location of McMurdo Sound in western Ross Sea adjacent to the northwestern corner of the Ross Ice Shelf and the Transantarctic Mountains. (b) Regional geologic map of area outline in part a. (Naish et al., 2007)

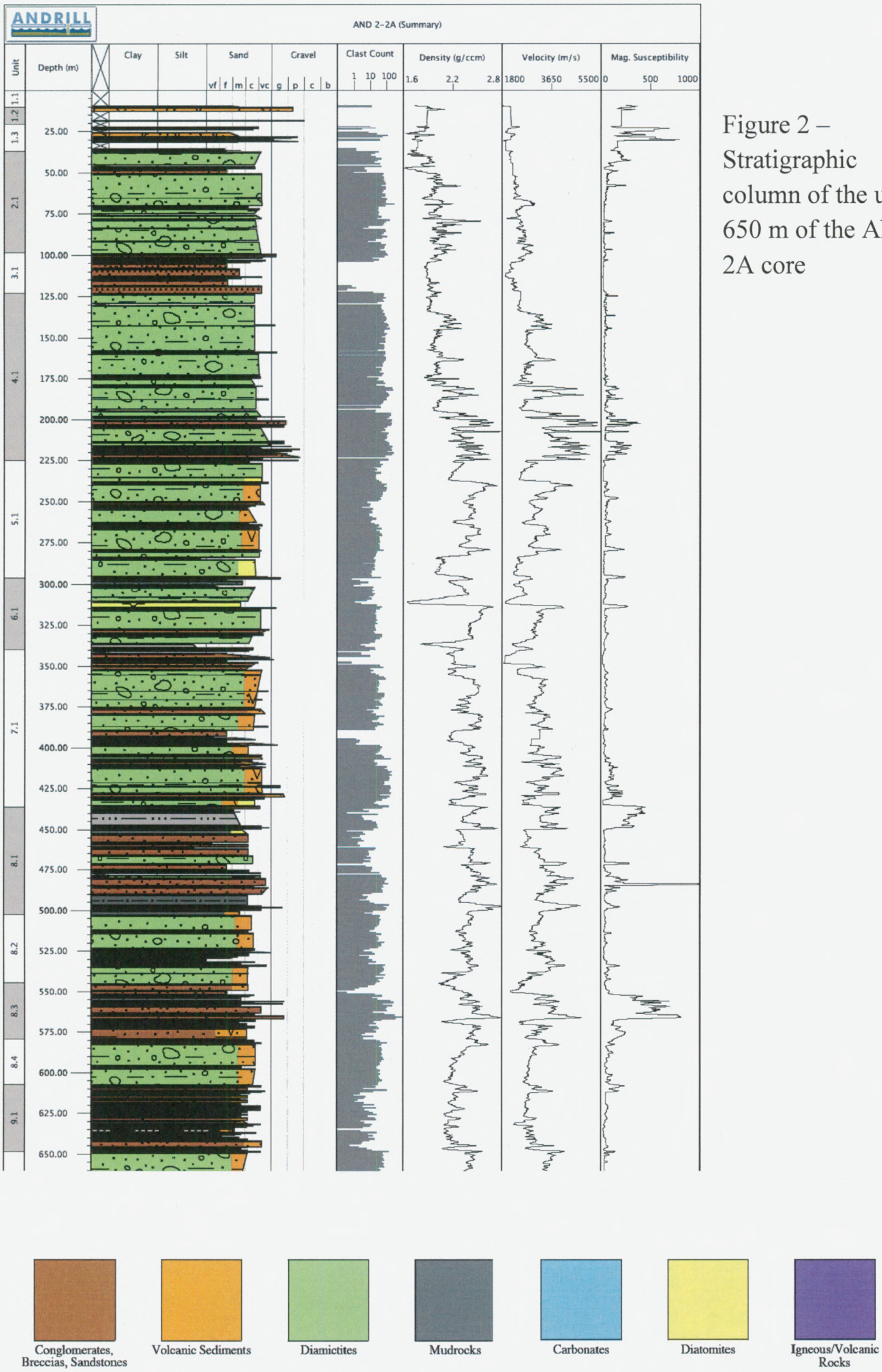

Figure 2 – Stratigraphic column of the upper 650 m of the AND-2A core

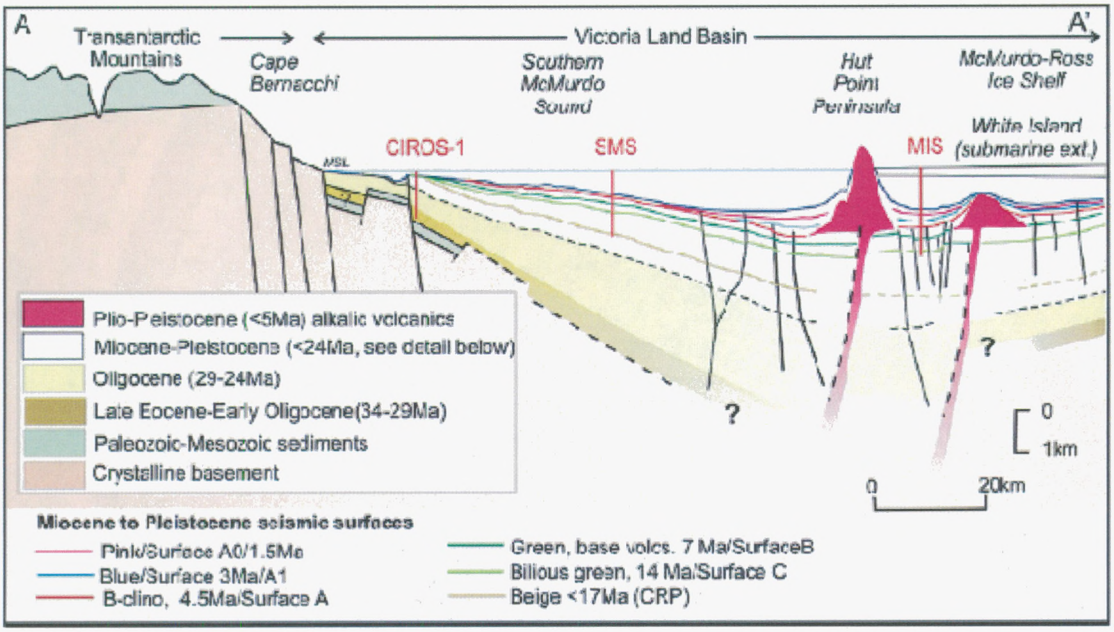
A
A'
Transantarctic Mountains
Victoria Land Basin
Cape Bernacchi
Southern McMurdo Sound
Hut Point Peninsula
McMurdo-Ross Ice Shelf
White Island (submarine ext.)
MSL
CIROS-1
SMS
MIS
?
?
0
1km
0
20km
Plio-Pleistocene (<5Ma) alkalic volcanics
Miocene-Pleistocene (<24Ma, see detail below)
Oligocene (29-24Ma)
Late Eocene-Early Oligocene(34-29Ma)
Paleozoic-Mesozoic sediments
Crystalline basement
Miocene to Pleistocene seismic surfaces
Pink/Surface A0/1.5Ma
Blue/Surface 3Ma/A1
B-clino, 4.5Ma/Surface A
Green, base volcs. 7 Ma/SurfaceB
Bilious green, 14 Ma/Surface C
Beige <17Ma (CRP)

Figure 3 - Geological cross-section of Southern McMurdo Sound showing seismic stratigraphy and structural geology (Naish *et al.,* 2006).

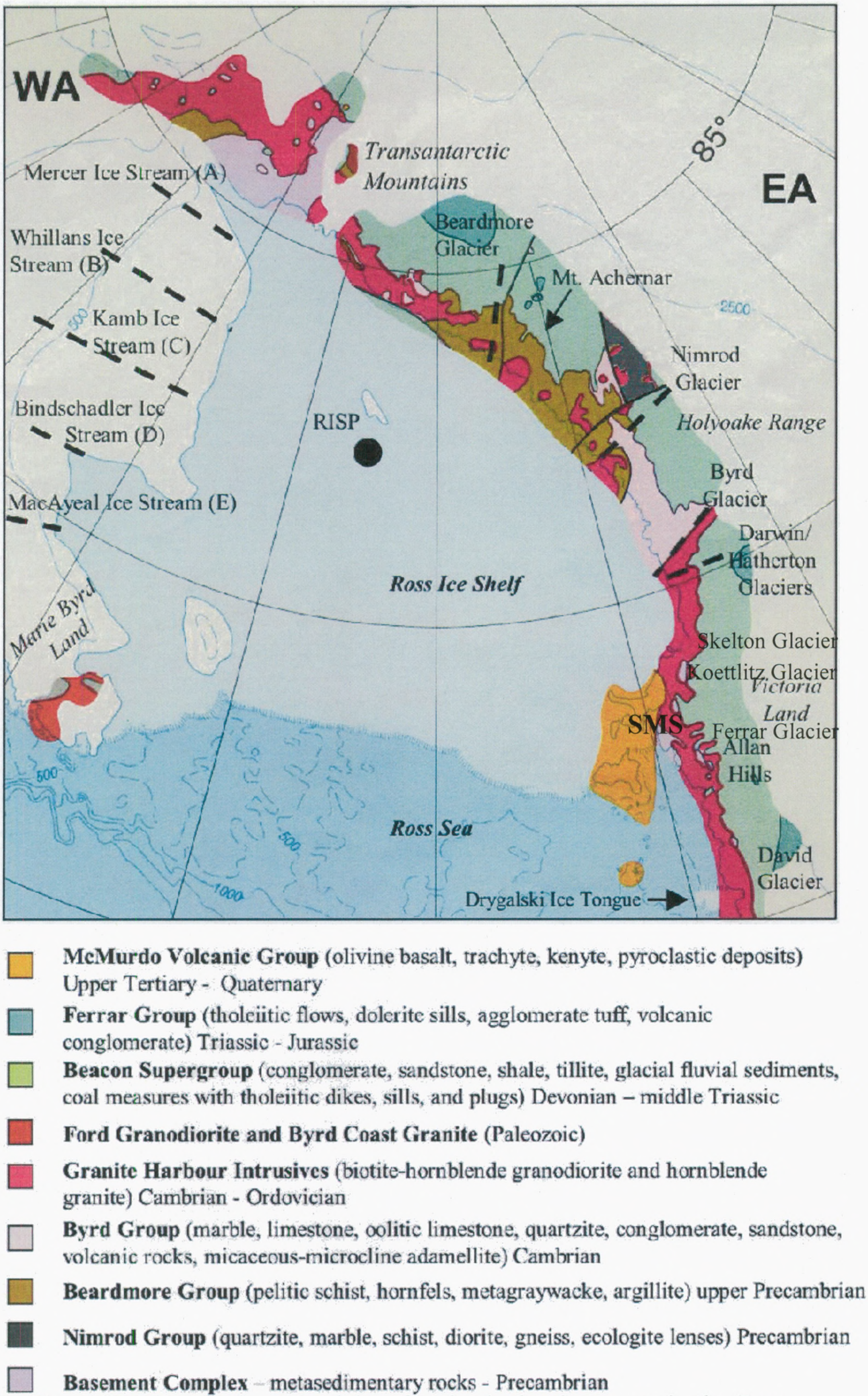
WA
EA
85°
Mercer Ice Stream (A)
Transantarctic Mountains
Whillans Ice Stream (B)
Beardmore Glacier
Mt. Achernar
2500
Kamb Ice Stream (C)
500
Nimrod Glacier
Holyoake Range
Bindschadler Ice Stream (D)
RISP
Byrd Glacier
MacAyeal Ice Stream (E)
Darwin/ Hatherton Glaciers
Ross Ice Shelf
Marie Byrd Land
Skelton Glacier
Koettlitz Glacier
Victoria Land
SMS
Ferrar Glacier
Allan Hills
500
Ross Sea
500
1000
David Glacier
Drygalski Ice Tongue

🟧 **McMurdo Volcanic Group** (olivine basalt, trachyte, kenyte, pyroclastic deposits) Upper Tertiary - Quaternary

🟦 **Ferrar Group** (tholeiitic flows, dolerite sills, agglomerate tuff, volcanic conglomerate) Triassic - Jurassic

🟩 **Beacon Supergroup** (conglomerate, sandstone, shale, tillite, glacial fluvial sediments, coal measures with tholeiitic dikes, sills, and plugs) Devonian – middle Triassic

🟥 **Ford Granodiorite and Byrd Coast Granite** (Paleozoic)

🟥 **Granite Harbour Intrusives** (biotite-hornblende granodiorite and hornblende granite) Cambrian - Ordovician

☐ **Byrd Group** (marble, limestone, oolitic limestone, quartzite, conglomerate, sandstone, volcanic rocks, micaceous-microcline adamellite) Cambrian

🟫 **Beardmore Group** (pelitic schist, hornfels, metagraywacke, argillite) upper Precambrian

⬛ **Nimrod Group** (quartzite, marble, schist, diorite, gneiss, ecologite lenses) Precambrian

🟪 **Basement Complex** – metasedimentary rocks - Precambrian

Figure 4 – Generalized geologic map of the of major bedrock sources in the Ross Embayment. Modified from Licht et al. (2005) from Bushnell and Craddock (1970).

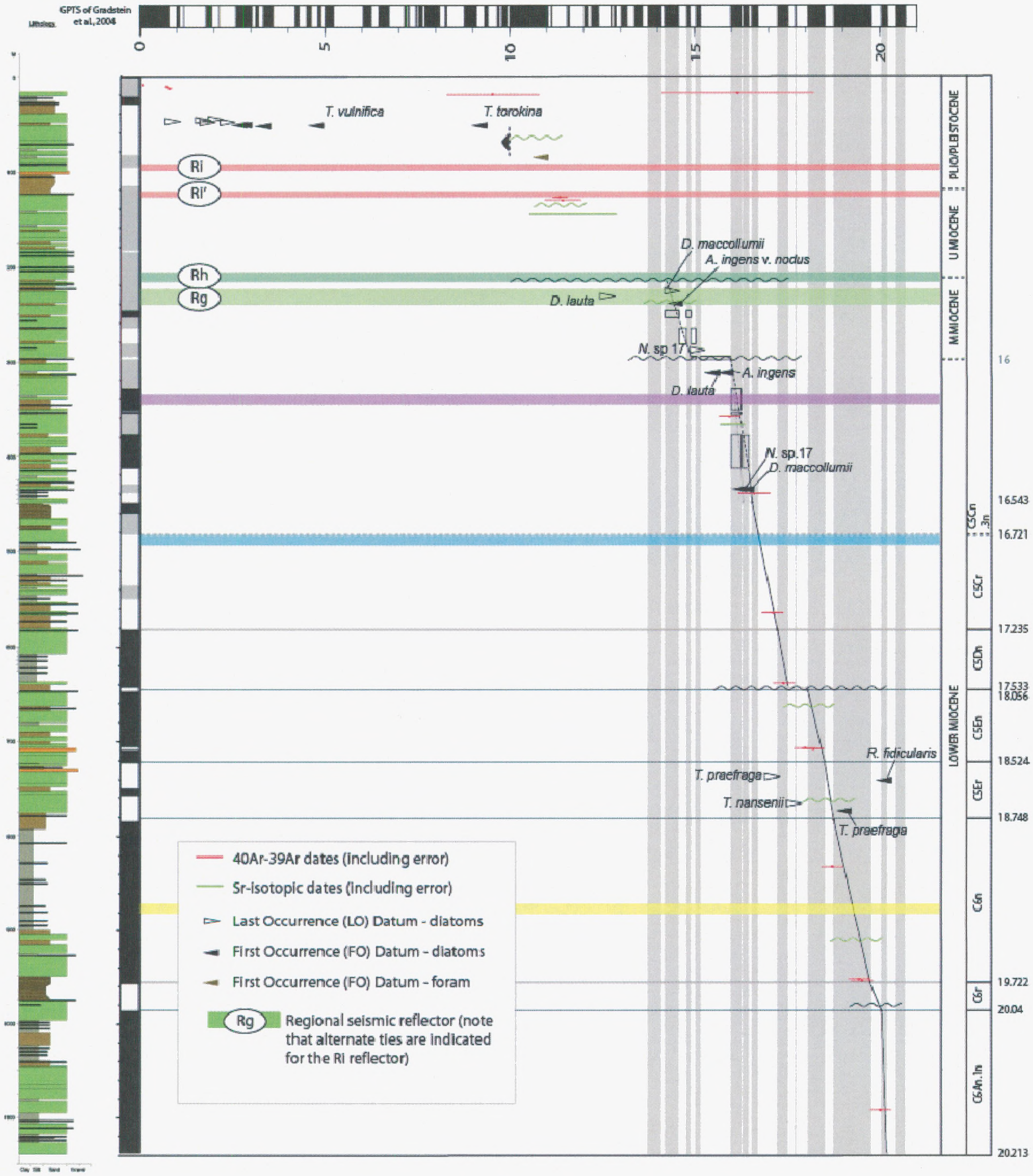

Figure 5 – Current integrated age model of the AND-2A core (ANDRILL SMS Science Team, 2010).

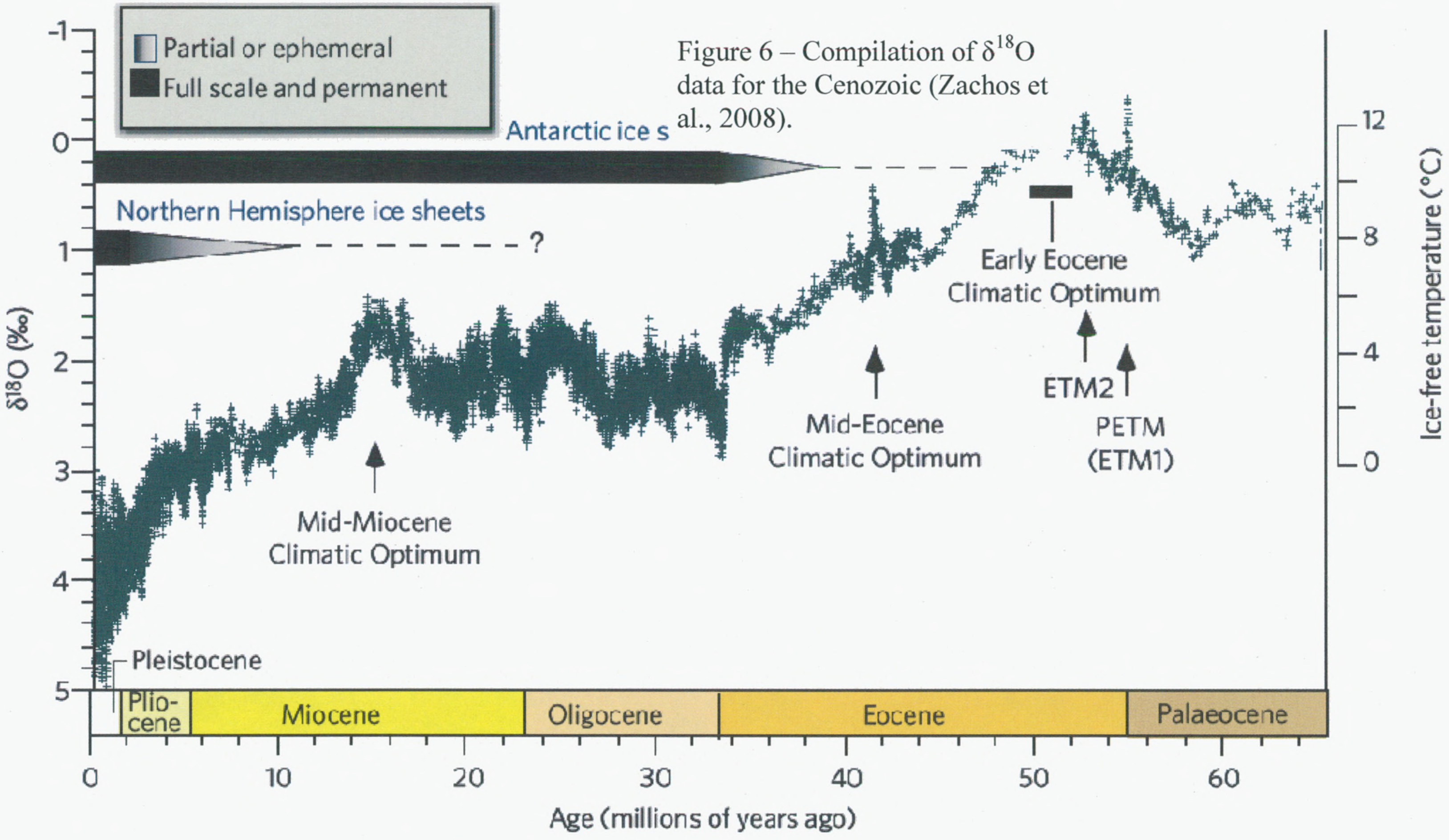

Figure 6 – Compilation of $\delta^{18}O$ data for the Cenozoic (Zachos et al., 2008).

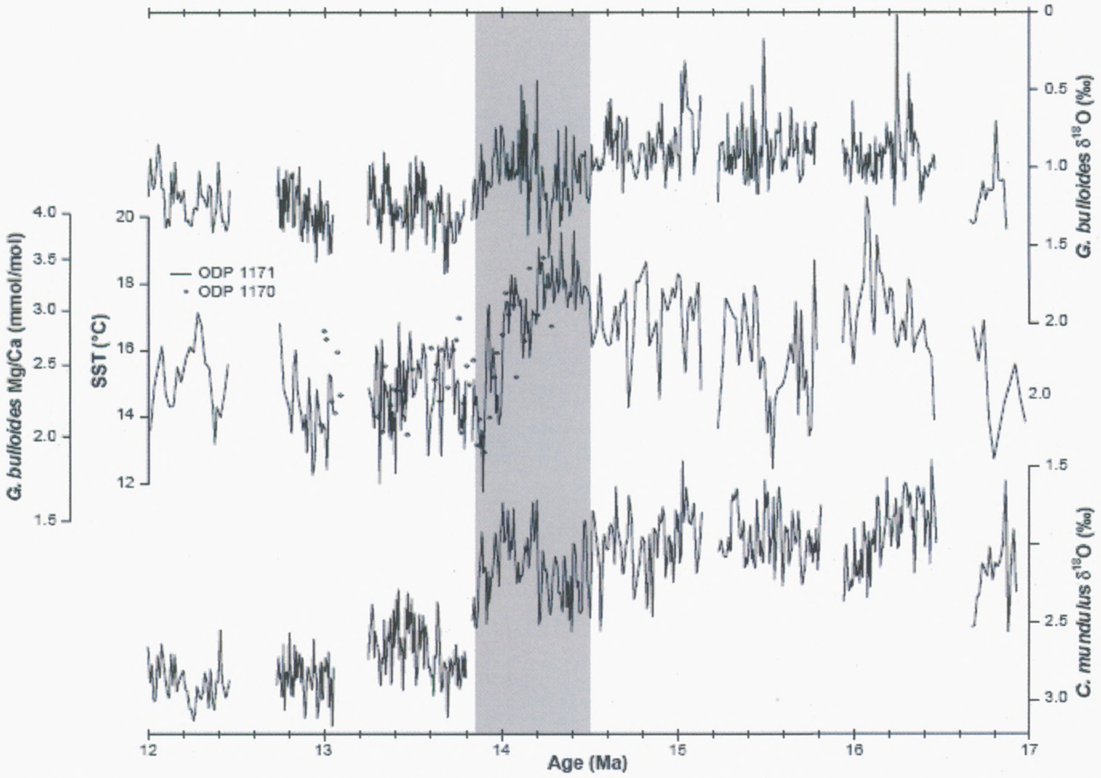

Figure 7 – Sea surface temperature (SST) and $\delta^{18}O$ showing the MMCT cooling period (Shevenell, 2004). The lower *C. mundulus* benthic foraminifer is used as a general proxy for Antarctic ice volume.

Figure 8 – Distribution of dominant heavy minerals.

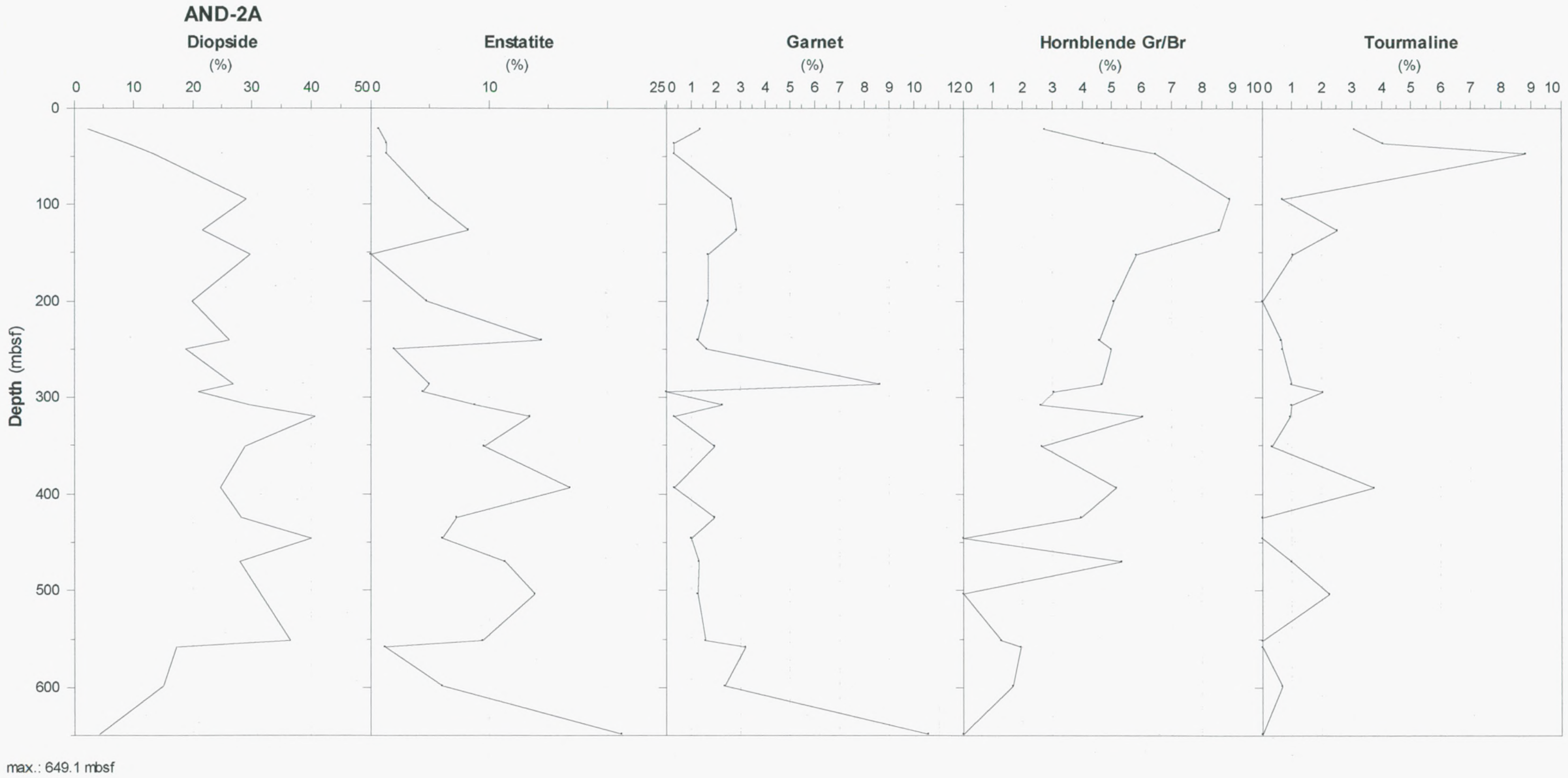

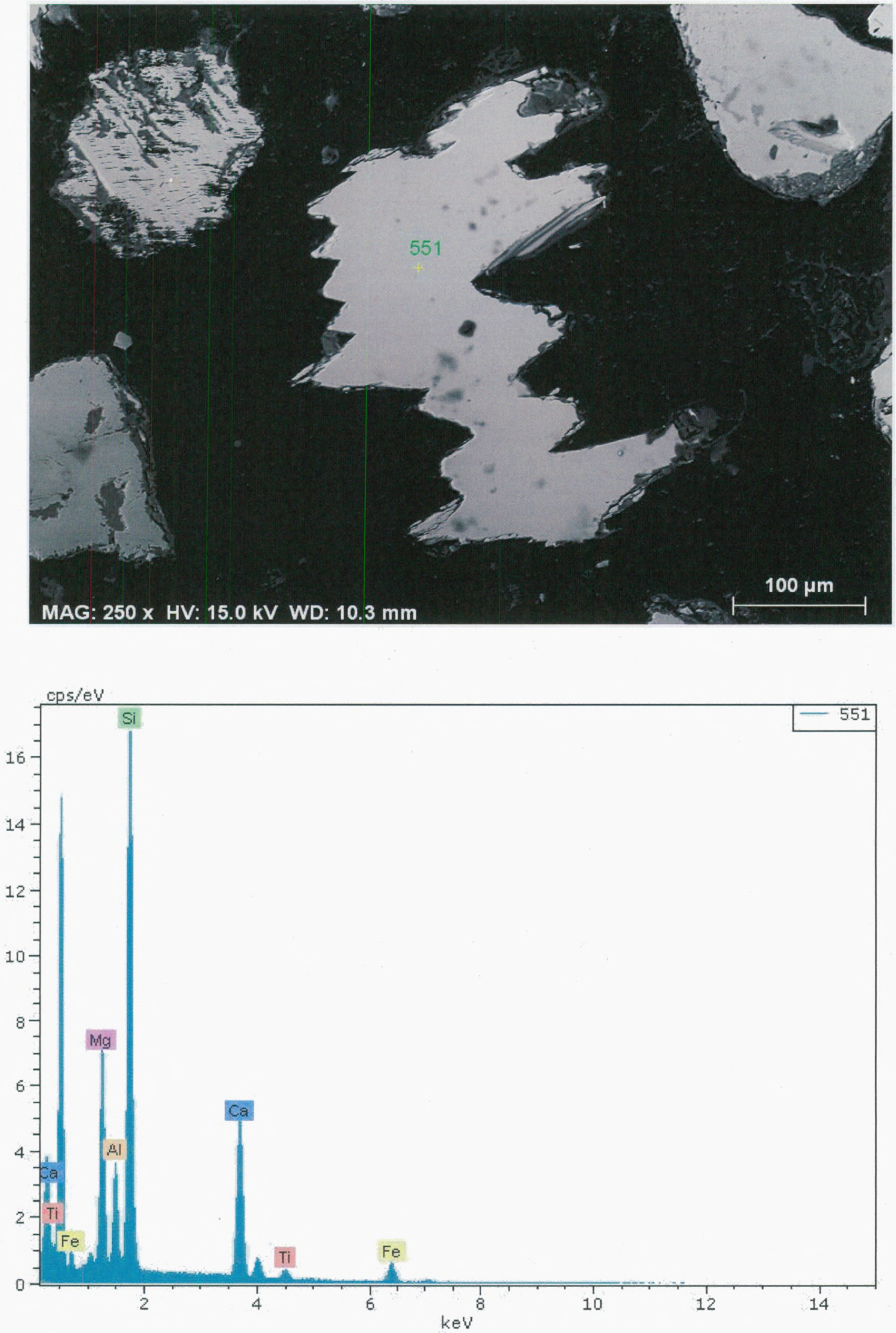

Figure 9 – SEM image of titanaugite and corresponding EDS detector spectra.

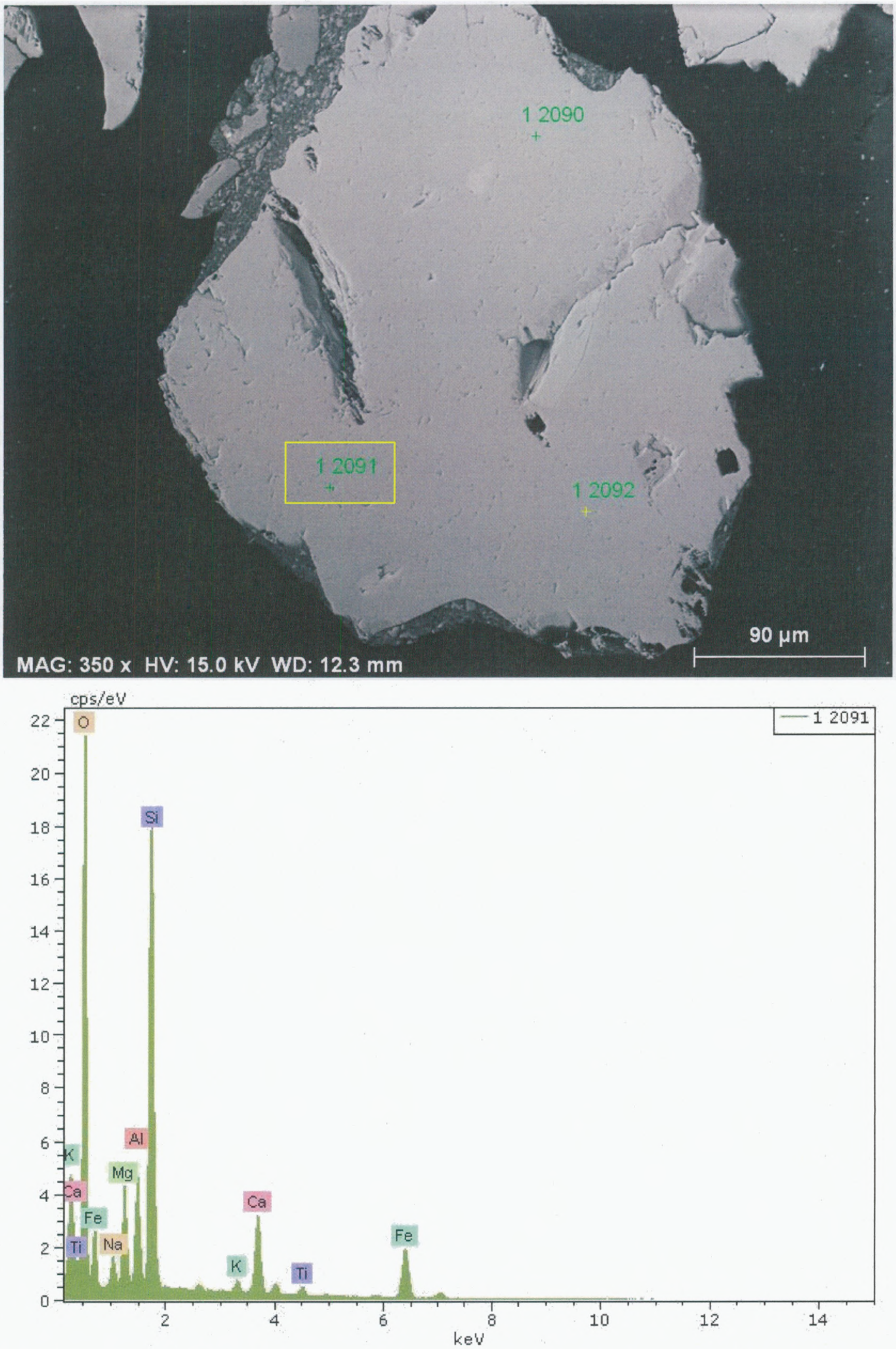

Figure 10 - Example SEM image (upper) and spectra (lower) of kaersutite (From sample 351.02 mbsf).

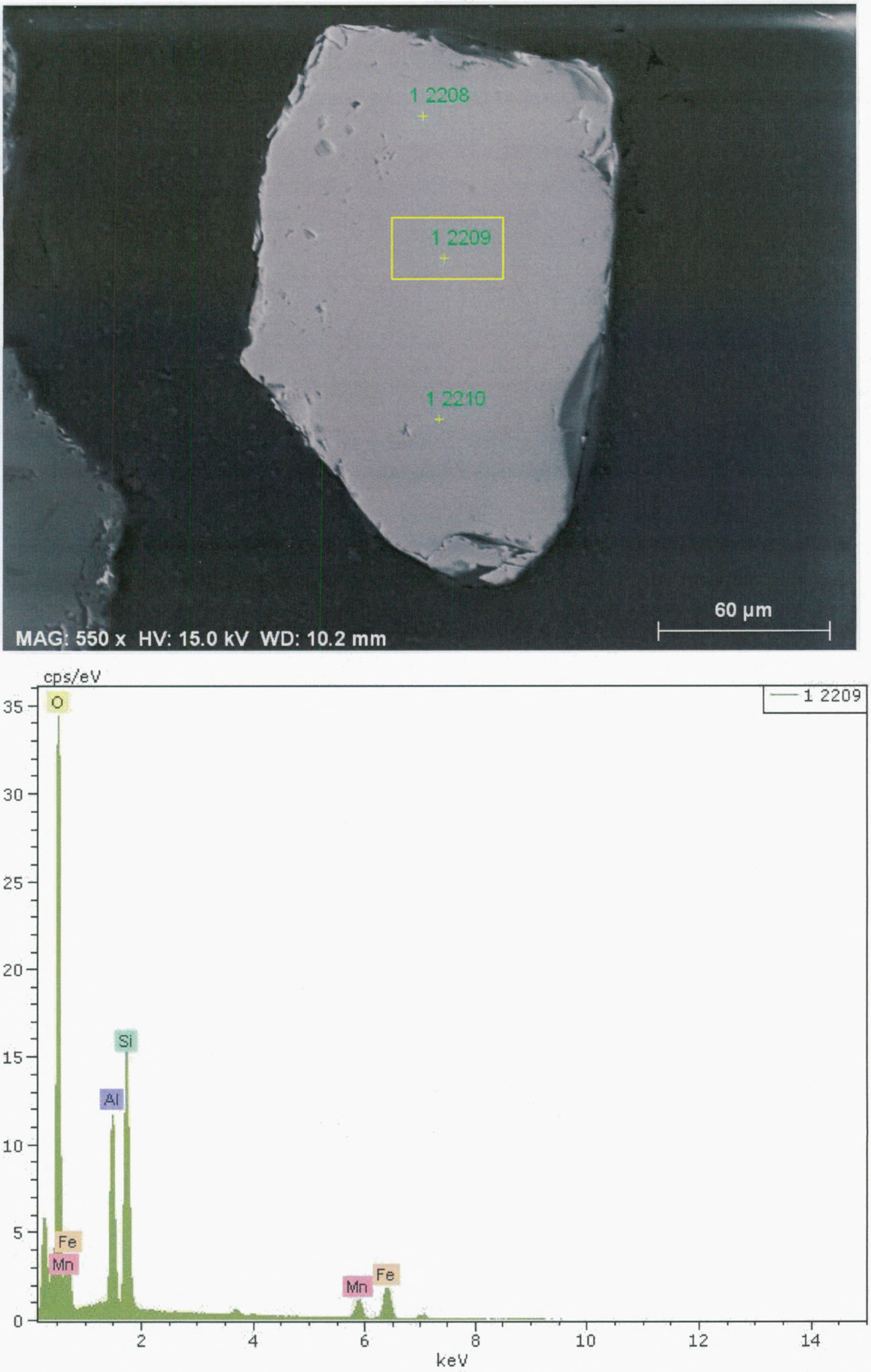

Figure 11 - Example SEM image (upper) and spectra (lower) of garnet (From sample 240.80 mbsf).

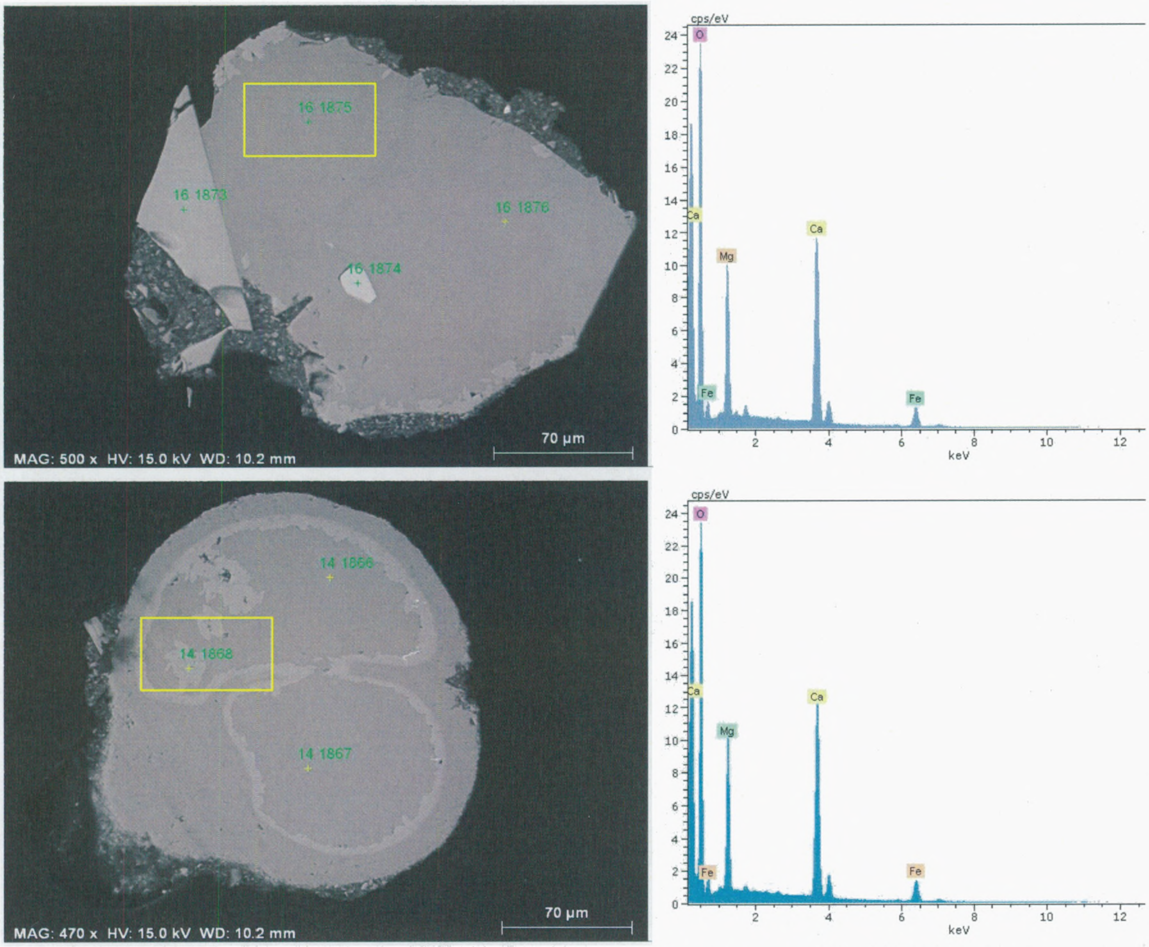

Figure 12 – Examples of dolomite SEM images with corresponding EDS detector spectra. Light grey and dark grey areas of the lower image are both dolomite.

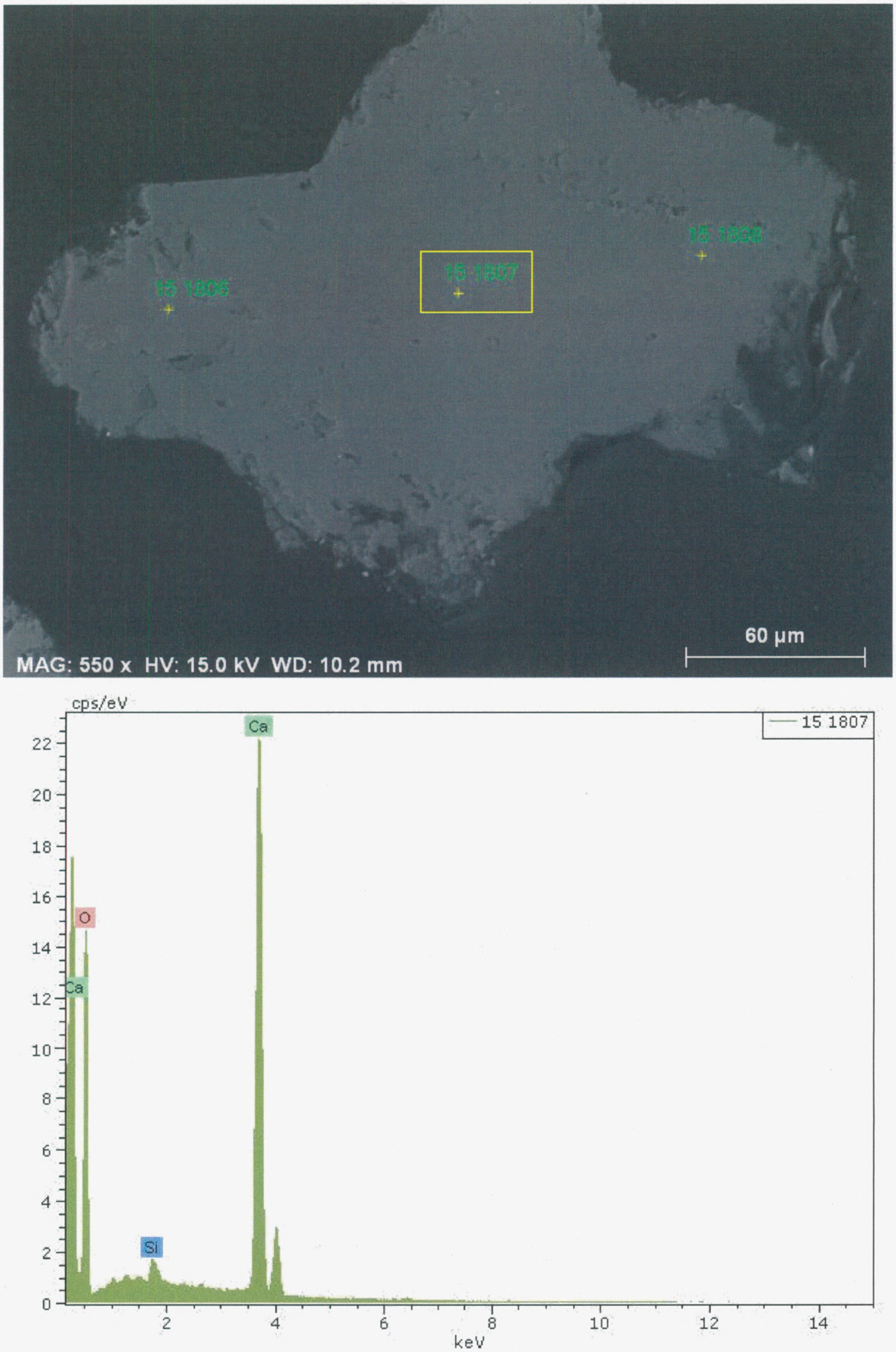

Figure 13 - Example SEM image (upper) and spectra (lower) of calcite (From sample 250.54 mbsf).

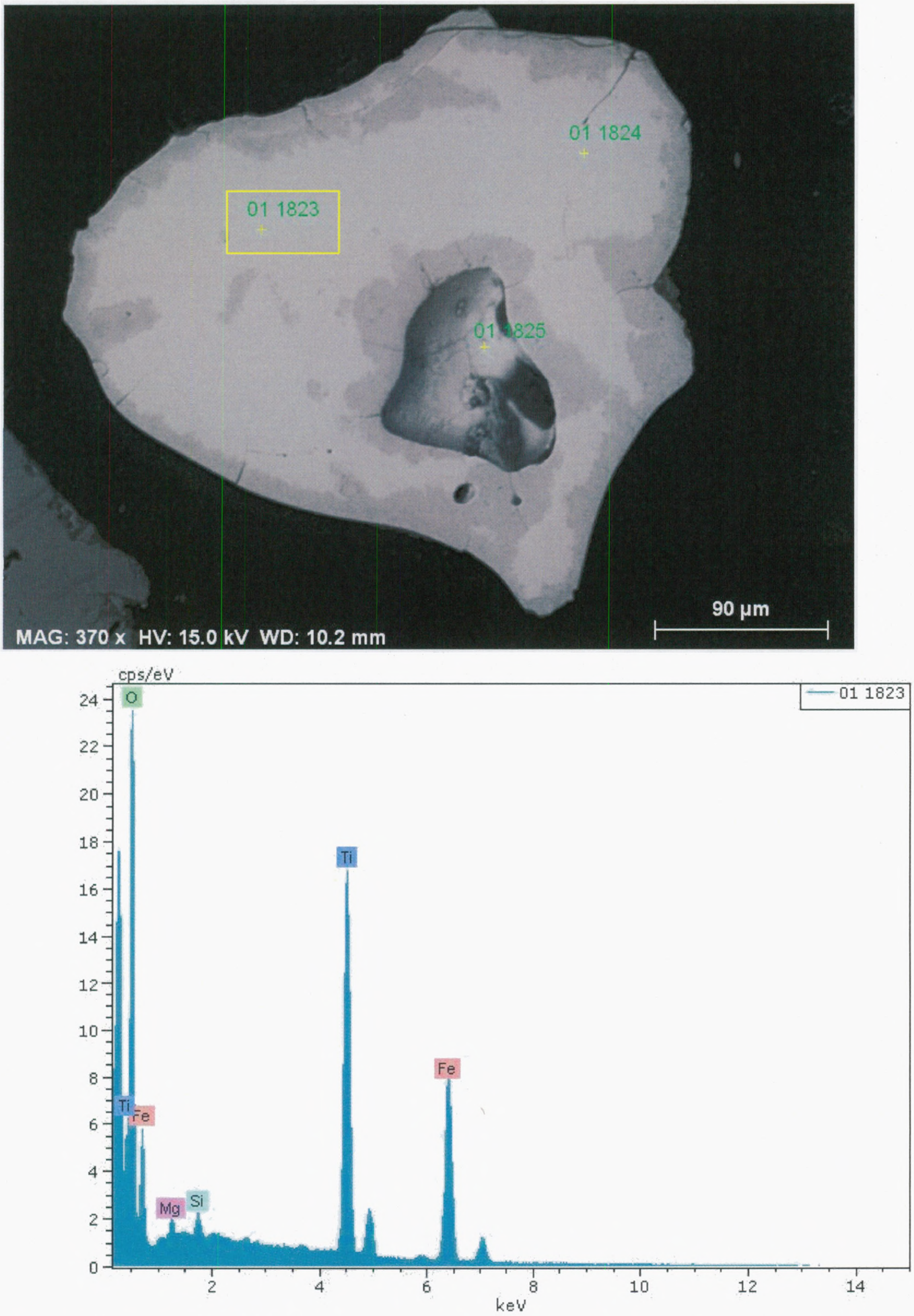

Figure 14 - Example SEM image (upper) and spectra (lower) of ilmenite (From sample 599.02 mbsf).

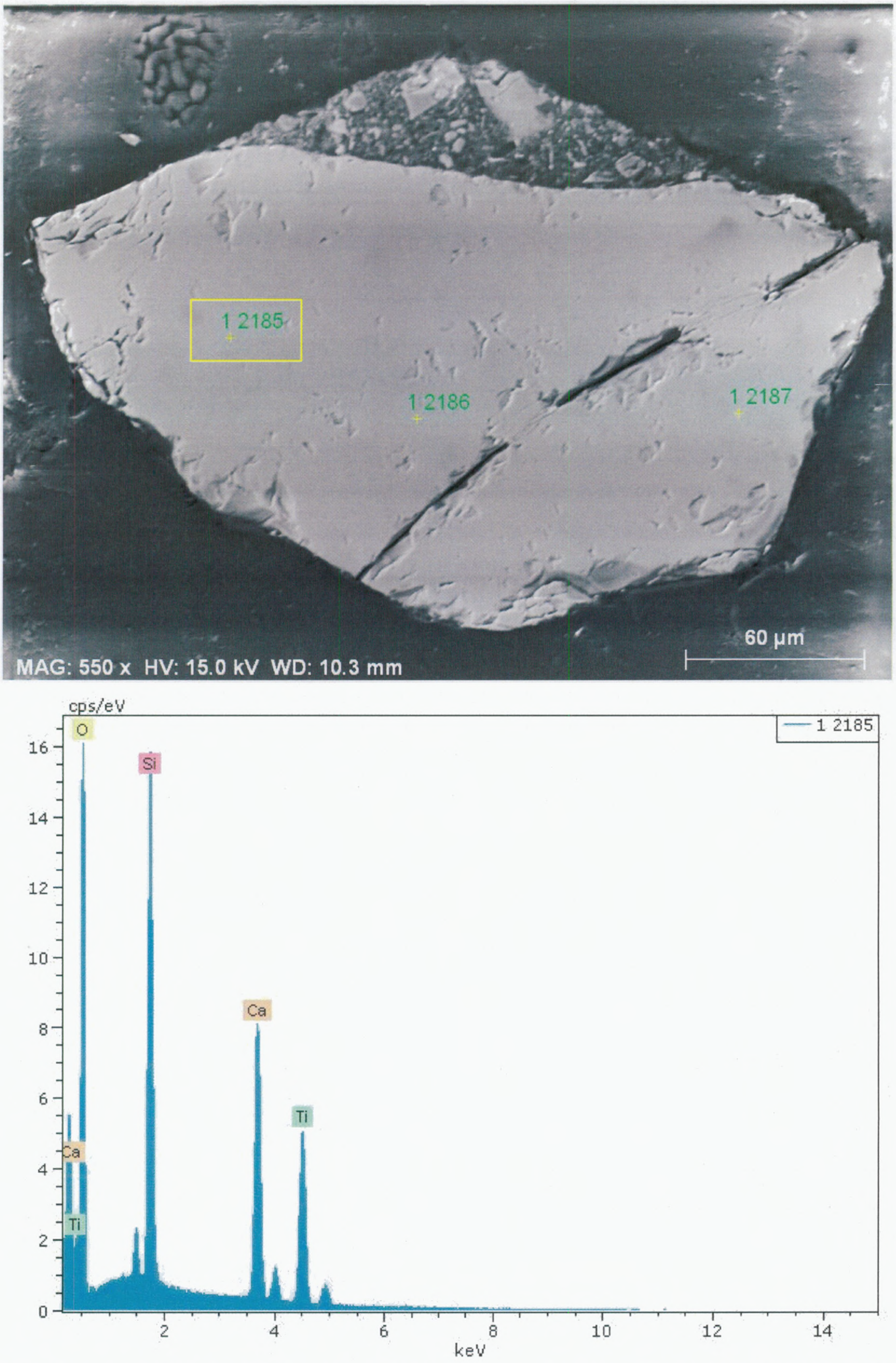

Figure 15 - Example SEM image (upper) and spectra (lower) of titanite/sphene (From sample 240.80 mbsf).

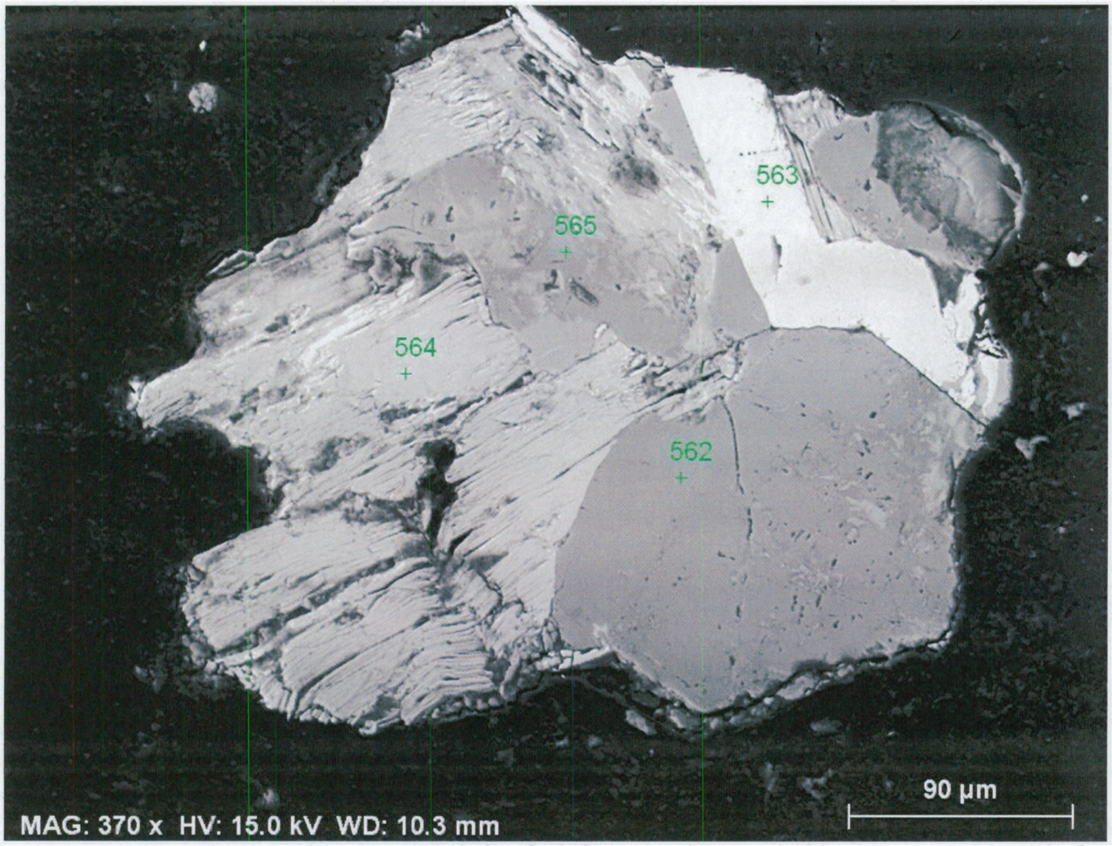
563
565
564
562
90 µm
MAG: 370 x HV: 15.0 kV WD: 10.3 mm

Figure 16 – Example SEM image of a rock fragment. 562/565 – Labradorite, 563 – Titanite/sphene, 564 – Stilpnomelane? (from sample 94.00 mbsf).

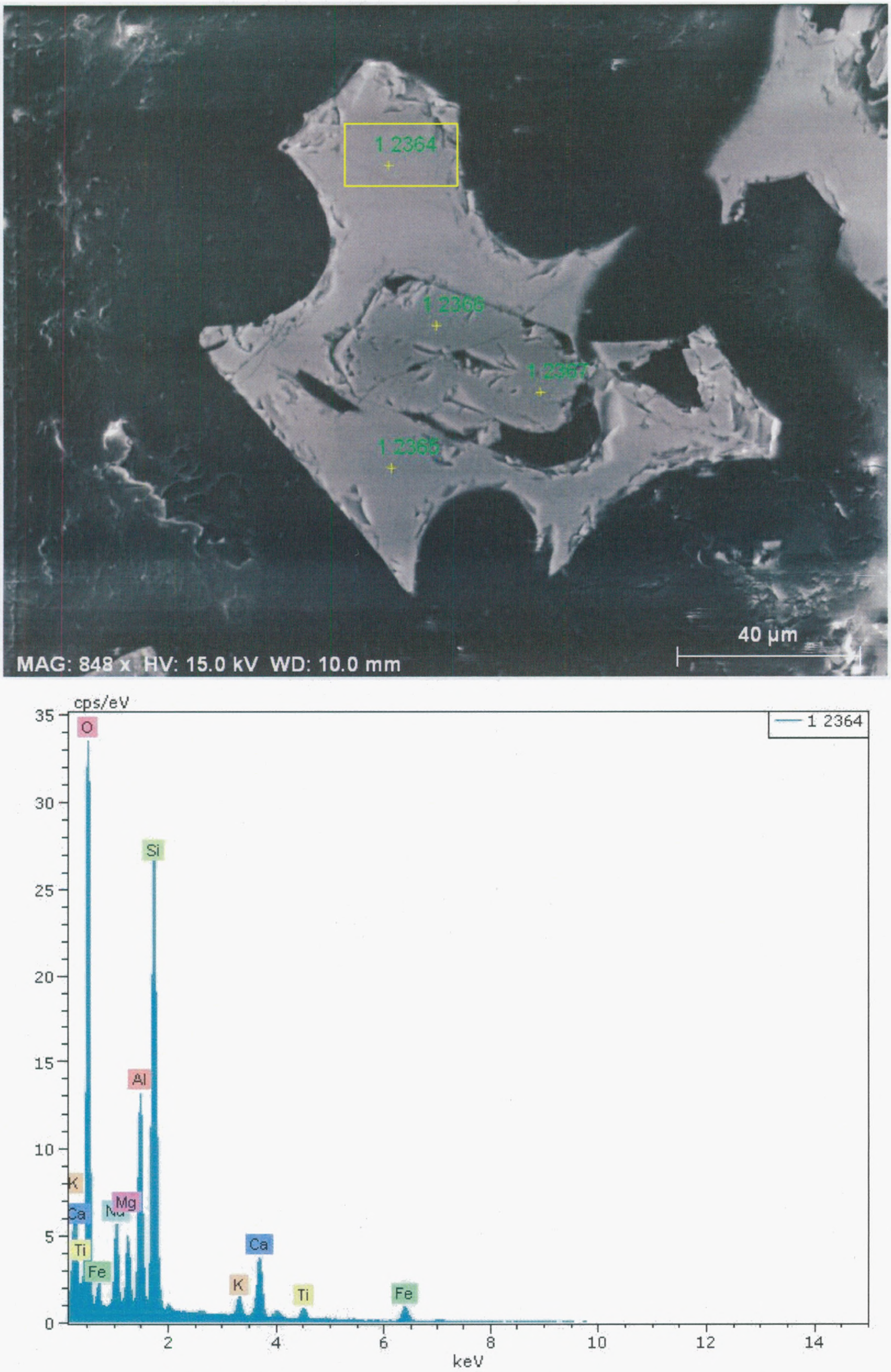

Figure 17 – Example SEM image (upper) and spectra (lower) of volcanic Glass with hornblende inclusion (From sample 36.74 mbsf).

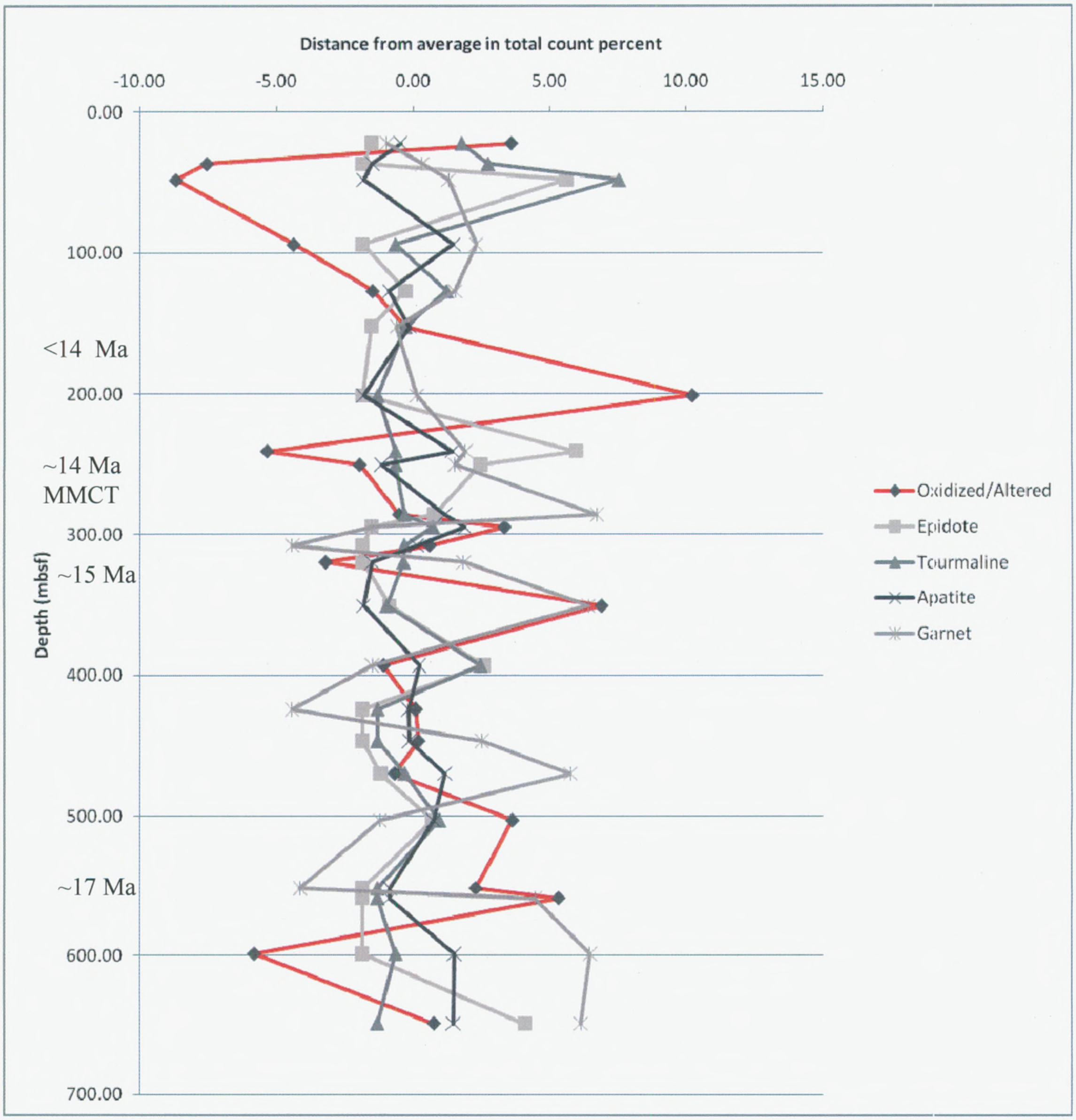

Figure 18 – Oxidized/altered, epidote, tourmaline, apatite, and garnet overlaid on a graph based on how far from the average count percentage the counts are at each depth. Oxidized/altered grains primarily do not come from a TAM source.

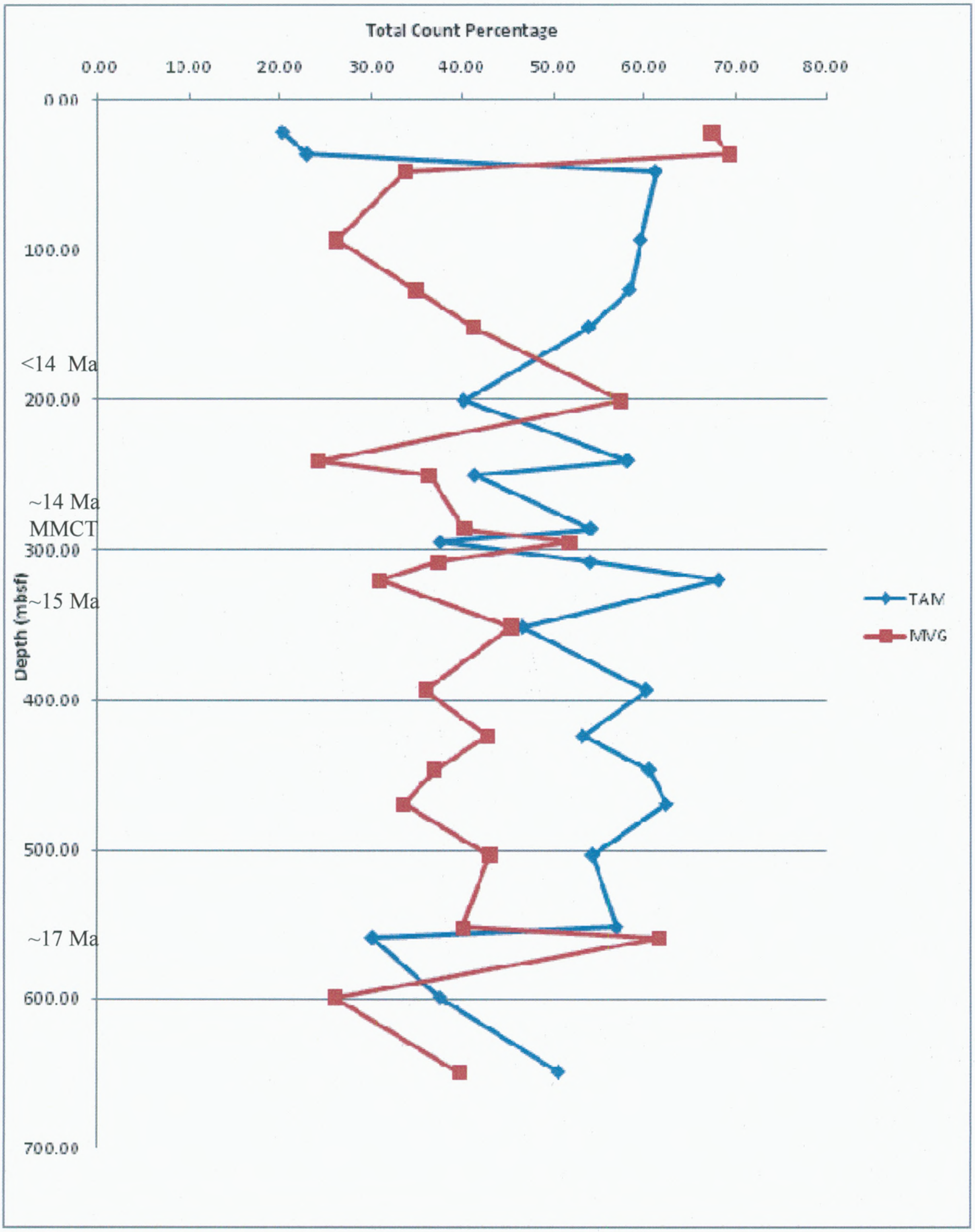

Figure 19 – Total count percentage of TAM vs. MVG.

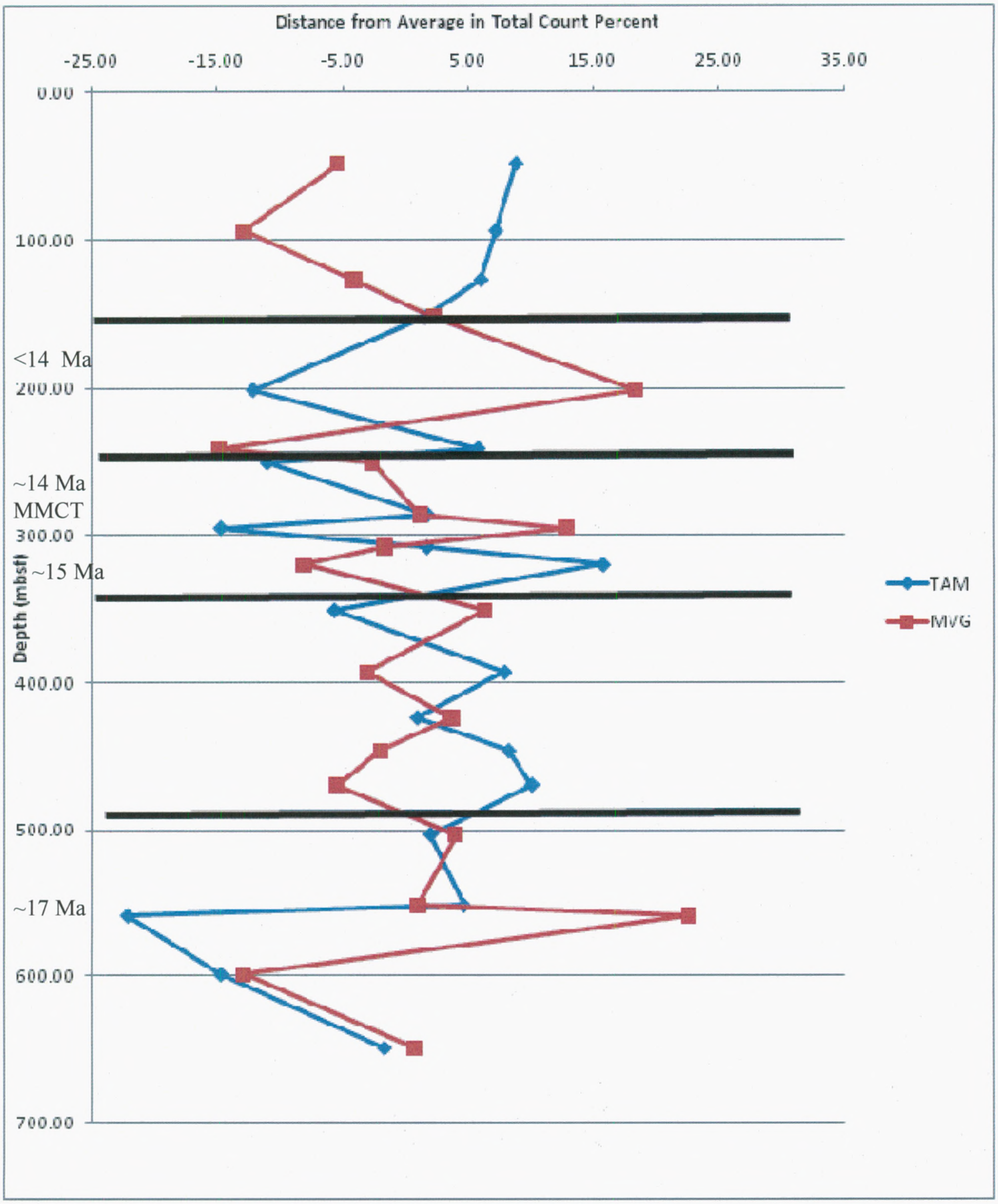

Figure 20 - TAM and MVG groups overlaid on a graph based on how far from the average count percentage the counts are at each depth. The MVG shows five different pulses of sediment input, denoted by the thick black lines.

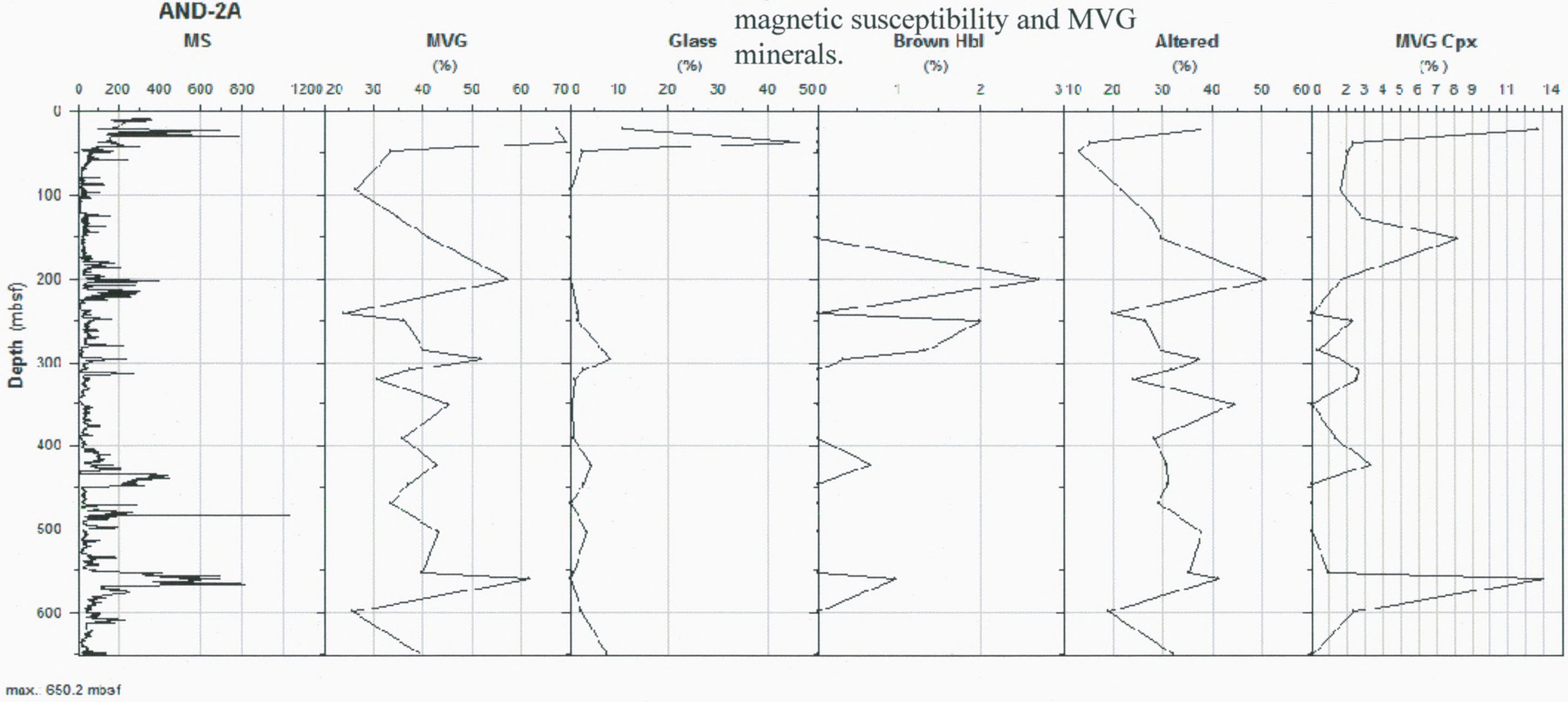

Figure 21 – Correlation between magnetic susceptibility and MVG minerals.

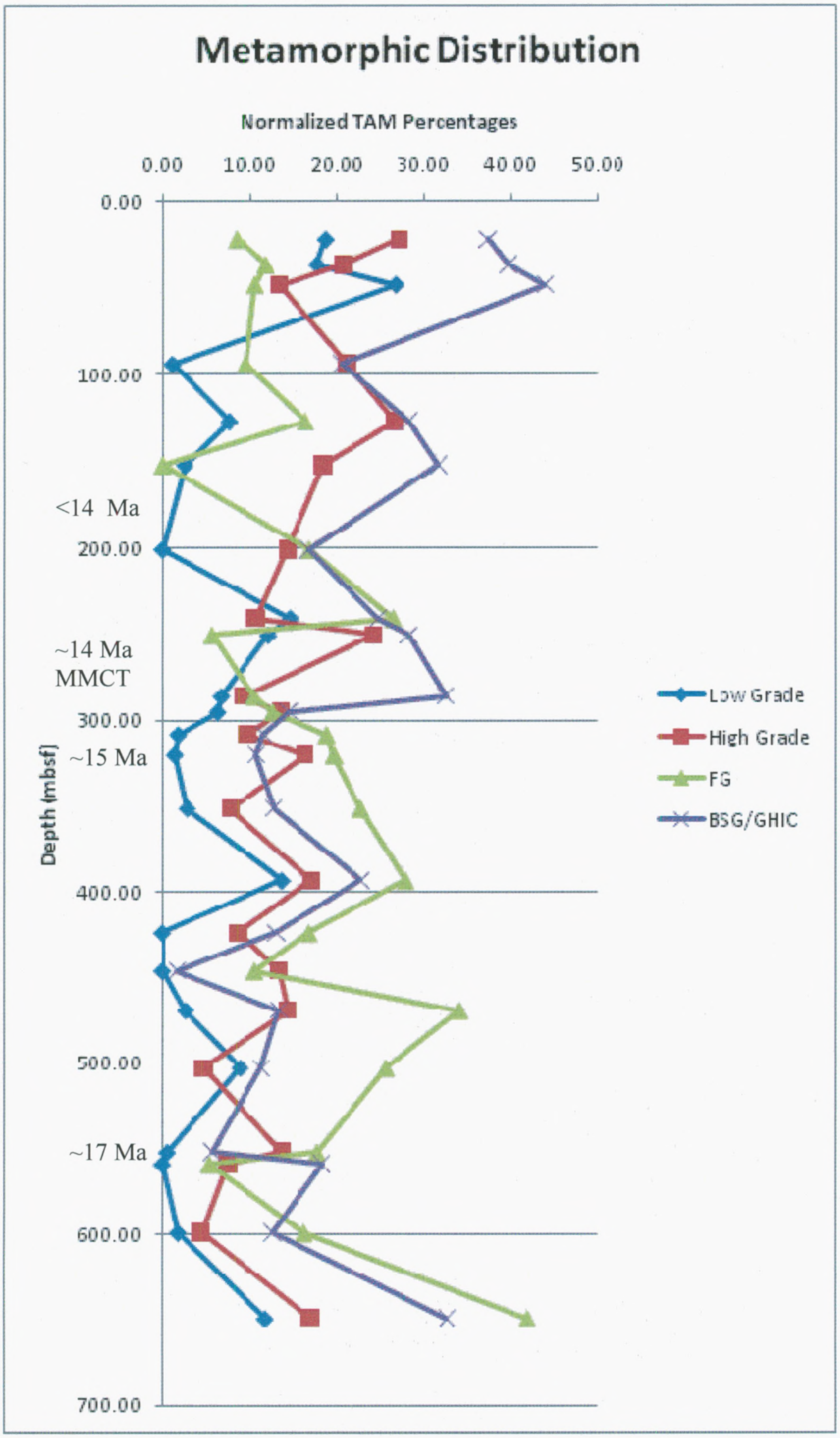

Figure 22 – TAM minerals broken down into source rock groups.

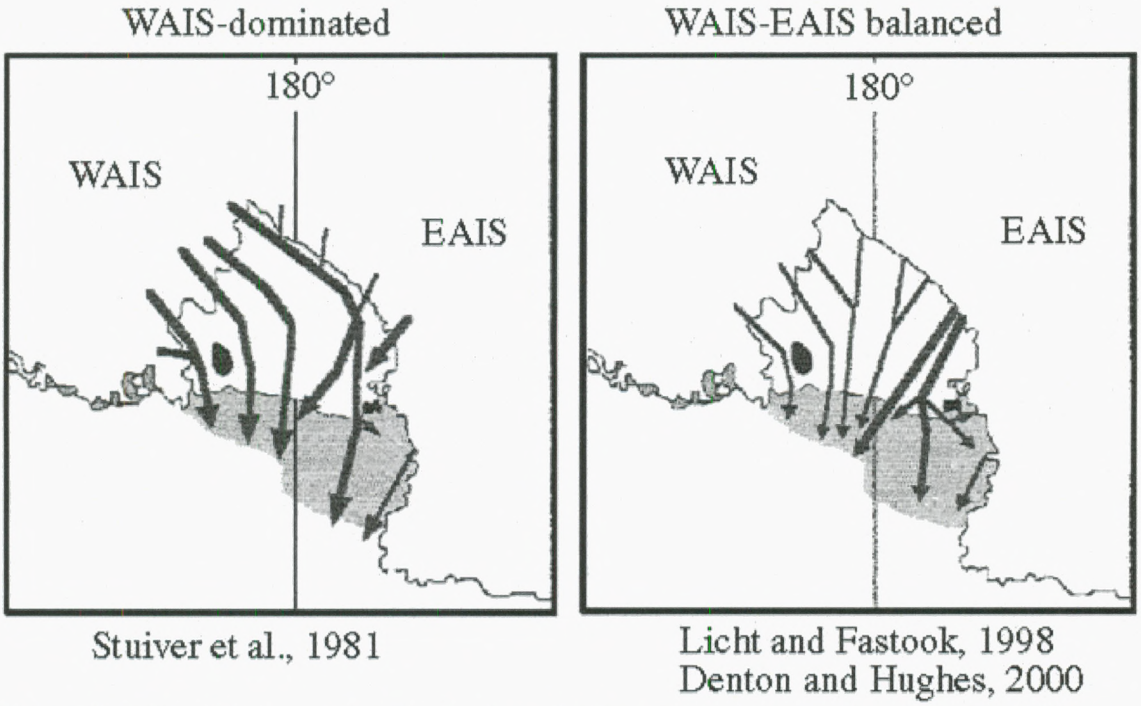
WAIS-dominated
180°
WAIS
EAIS
WAIS-EAIS balanced
180°
WAIS
EAIS

Stuiver et al., 1981

Licht and Fastook, 1998
Denton and Hughes, 2000

Figure 23 – Possible scenarios for ice sheet drainage dependent on the size of the WAIS (Licht et al., 2005).

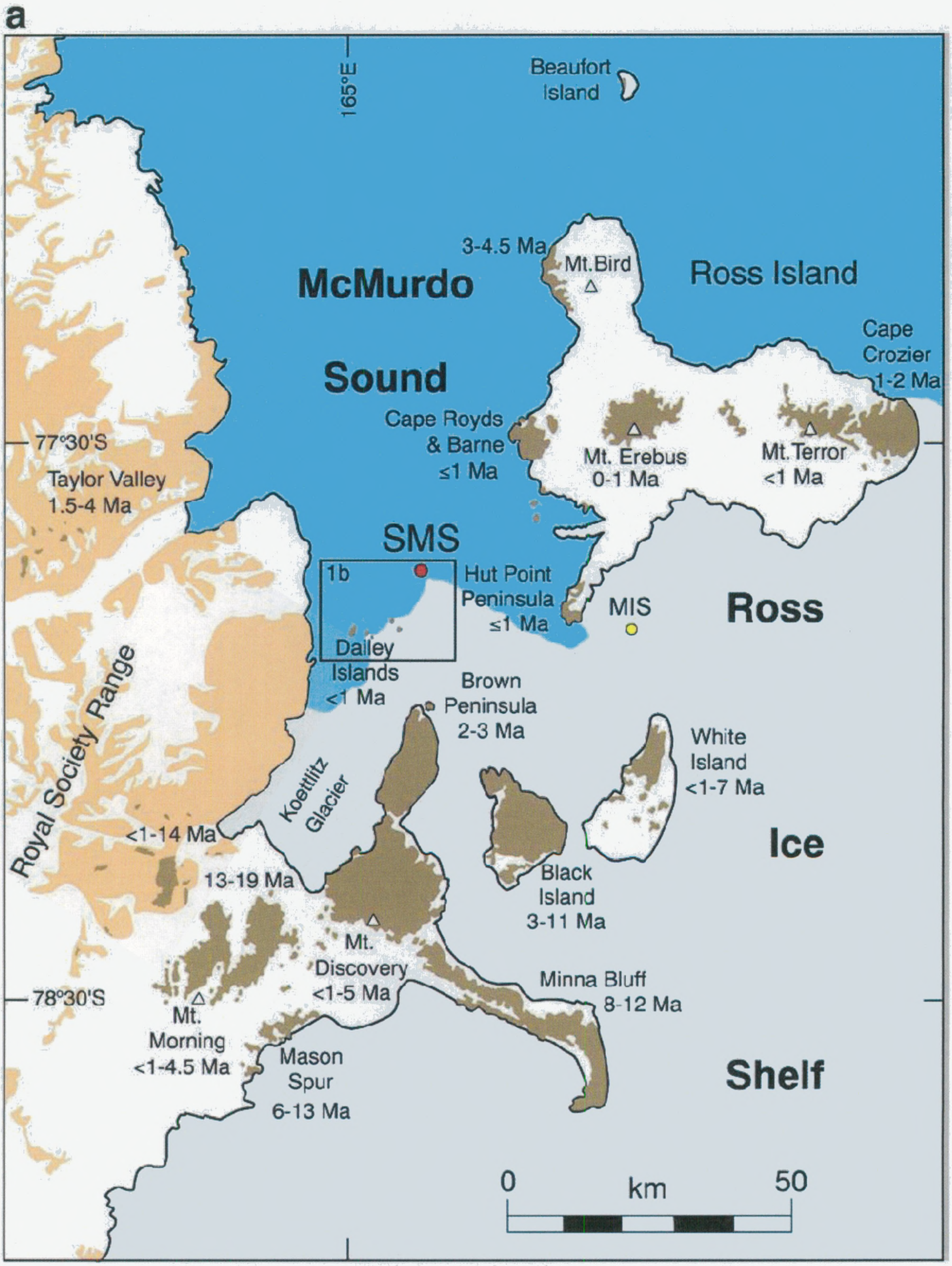
a
165°E
Beaufort Island
3-4.5 Ma
Mt. Bird
Ross Island
McMurdo
Sound
Cape Crozier
1-2 Ma
Cape Royds & Barne
≤1 Ma
Mt. Erebus
0-1 Ma
Mt. Terror
<1 Ma
77°30'S
Taylor Valley
1.5-4 Ma
SMS
1b
Hut Point Peninsula
≤1 Ma
MIS
Ross
Dailey Islands
<1 Ma
Brown Peninsula
2-3 Ma
White Island
<1-7 Ma
Royal Society Range
Koettlitz Glacier
<1-14 Ma
Ice
13-19 Ma
Black Island
3-11 Ma
Mt. Discovery
<1-5 Ma
Minna Bluff
8-12 Ma
78°30'S
Mt. Morning
<1-4.5 Ma
Mason Spur
6-13 Ma
Shelf
0
km
50

Figure 24 - Map of McMurdo Sound area showing the ANDRILL SMS and MIS drill-sites relative to exposed deposits of the Erebus Volcanic Province (Del Carlo et al., 2009).

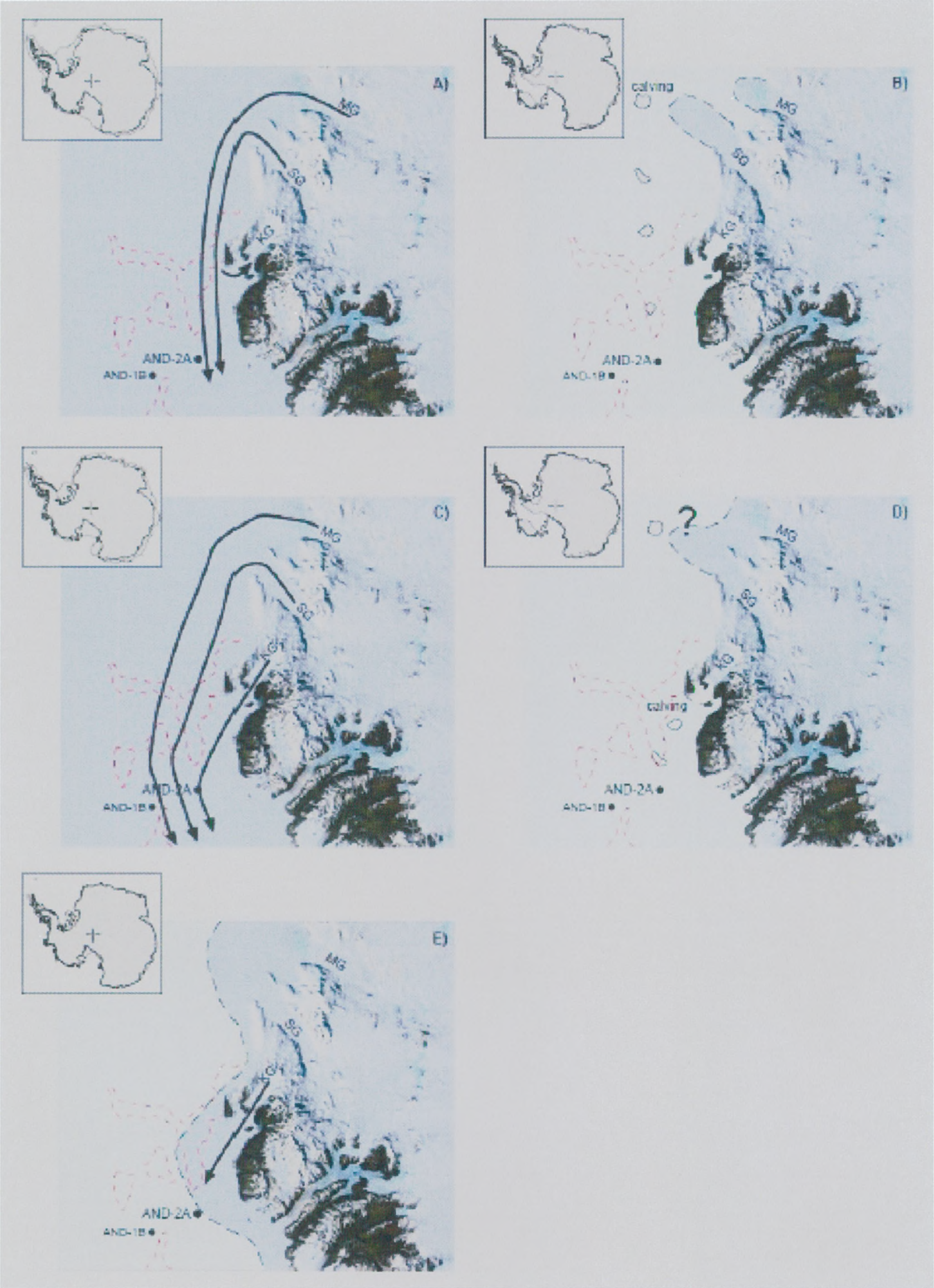
A)
MG
SG
KG
AND-2A
AND-1B
B)
calving
MG
SG
KG
AND-2A
AND-1B
C)
MG
SG
KG
AND-2A
AND-1B
D)
?
MG
SG
KG
calving
AND-2A
AND-1B
E)
MG
SG
KG
AND-2A
AND-1B

Figure 25 - Paleo-glacial-flow patterns occurring in the McMurdo Sound during the late Early-Late Miocene. A) Maximum ice-sheet expansion, consistent with the Skelton-sourced domains occurring below ca. 626 mbsf. B) Interglacial setting explaining the occurrences of Skelton-sourced ice-rafted debris in the ca. 503-488 mbsf interval. C) An Antarctic ice sheet partly reduced within the Ross Embayment above 225 mbsf. D) Interglacial setting explaining the occurrences of Koettlitz-sourced ice-rafted debris above ca. 625 mbsf. E) Reconstructed glacial setting for AND-2B glacial sediments in the ca. 626-503 mbsf and ca. 488-225 mbsf intervals (from Sandroni et al., 2010). Abbreviations: MG Mulock Glacier; SG Skelton Glacier; KG Koettlitz Glacier.

Tables

Sample (mbsf)	Original Weight (g)	63-250 µm Weight (g)	Light Fraction Weight (g)	Heavy Fraction Weight (g)	% or Sample
22.13-22.14	8.1012	1.4010	1.2677	0.1163	1.436
28.22-28.24	9.4725	0.0360	0.0315	0.0010	0.011
36.74-36.75	7.6980	1.6750	1.6447	0.0109	0.142
48.27-48.28	13.4834	0.9905	0.8959	0.0772	0.573
94.00-94.01	12.5501	3.2134	2.9029	0.2716	2.164
126.98-127.00	7.7957	1.0221	0.9883	0.0338	0.434
152.01-152.02	11.9760	2.2404	2.0999	0.1296	1.082
201.01-201.02	11.5315	2.8752	2.5369	0.2799	2.427
240.80-240.82	16.2634	3.8888	3.6295	0.2593	1.594
250.54-250.56	13.0866	3.0443	2.7890	0.2328	1.779
285.01-285.03	11.2094	2.5274	2.3182	0.2092	1.866
295.04-295.06	10.1759	5.2347	4.7865	0.4846	4.762
308.01-308.03	12.6870	1.3723	1.2958	0.0765	0.603
319.96-319.98	10.2428	3.7644	3.5264	0.2380	2.324
351.02-351.04	12.1723	3.0909	2.9028	0.2041	1.677
393.00-393.02	10.4175	7.2195	7.2136	0.2418	2.321
422.96-422.98	11.8607	4.1099	3.7653	0.3446	2.905
446.38-446.40	11.7863	3.2951	2.8717	0.3399	2.884
469.48-469.50	12.9388	4.5262	4.4188	0.1074	0.830
503.00-503.01	11.9815	2.9488	2.7867	0.1236	1.032
551.99-552.00	11.8368	4.8706	4.4715	0.3186	2.692
559.00-559.01	13.5978	4.4751	4.4741	0.1599	1.176
599.02-599.04	12.1826	1.6956	1.6214	0.0742	0.609
649.10-649.11	10.1574	2.4810	2.2094	0.2716	2.674

Table 1 – Sample depths chosen for heavy mineral separation and weights throughout the procedure.

Table 2 – Count percentages of the most common and useful heavy minerals.

Depth (mbsf)	22.14	36.74	48.27	94.00	126.98	152.01	201.01	240.80	250.54	286.01	295.04	308.01	319.96	351.02	393.00	423.96	446.38	469.48	503.00	551.99	559.00	599.02	649.10
Apatite	1.37	0.34	0.00	3.31	0.95	1.71	0.00	3.27	0.67	2.99	3.73	1.97	0.32	0.00	2.05	1.66	1.68	2.99	2.59	0.98	0.97	3.39	3.31
Augite, brown	12.71	1.35	2.04	1.66	1.90	8.19	0.00	0.00	1.00	0.00	0.00	0.33	0.96	0.00	0.00	0.00	0.00	0.00	0.00	0.00	12.66	1.36	0.00
Augite, green	2.41	2.36	3.06	8.94	2.86	2.73	6.08	0.65	3.67	3.65	3.39	4.59	1.27	0.33	0.00	0.99	0.00	1.00	0.32	0.65	5.52	0.34	0.00
Augite, green/brown	2.75	0.00	9.86	0.00	0.00	0.00	0.00	0.00	0.00	0.00	0.00	0.00	0.00	0.00	0.00	7.28	5.05	0.00	0.00	0.00	0.00	0.00	0.00
Augite, red/purple	0.00	1.01	0.00	0.00	0.95	0.00	1.69	0.00	1.33	0.33	1.69	2.30	1.59	0.00	1.37	3.31	0.00	0.00	0.00	0.98	0.32	1.02	0.00
Augite, red/pink	5.84	4.73	15.31	2.65	4.44	3.07	1.69	2.61	3.67	1.99	4.41	0.00	3.18	0.66	5.48	3.64	3.03	4.32	1.62	3.26	6.49	2.03	0.00
Clinozoisite	0.00	0.00	7.48	0.00	0.00	0.34	0.00	7.84	4.33	2.66	0.00	0.00	0.00	0.00	2.74	0.00	0.00	0.00	2.59	0.00	0.00	0.00	0.00
Diopside	2.41	8.78	13.27	29.14	21.59	29.69	19.93	26.14	18.67	26.91	21.02	29.51	40.76	28.81	24.66	28.15	40.07	27.91	31.39	36.48	17.21	14.92	4.30
Enstatite	0.69	1.35	1.36	4.97	8.25	0.00	4.73	14.38	2.00	4.98	4.41	8.85	13.38	9.60	16.78	7.28	6.06	11.30	13.92	9.45	1.30	6.10	21.19
Epidote	0.34	0.00	0.00	0.00	1.59	0.00	0.00	0.00	0.00	0.00	0.34	0.00	0.00	0.99	1.71	0.00	0.00	0.66	0.00	0.00	0.00	0.00	5.96
Garnet	1.37	0.34	0.34	2.65	2.86	1.71	1.69	1.31	1.67	8.64	0.00	2.30	0.32	1.99	0.34	1.99	1.01	1.33	1.29	1.63	3.25	2.37	10.60
Glass w/inclusions	11.00	46.62	2.72	0.00	0.00	0.00	0.00	1.63	1.67	6.98	8.14	2.95	0.96	0.33	0.68	4.30	3.03	0.00	3.56	0.65	0.00	2.37	7.62
Hornblende br	0.00	0.00	0.00	0.00	0.00	0.00	2.70	0.00	2.00	1.33	0.34	0.00	0.00	0.00	0.00	0.66	0.00	0.00	0.00	0.00	0.97	0.00	0.00
Hornblende gr/br	2.75	4.73	6.46	8.94	8.57	5.80	5.07	4.58	5.00	4.65	3.05	2.62	6.05	2.65	5.14	3.97	0.00	5.32	0.00	1.30	1.95	1.69	0.00
Hypersthene	1.03	1.35	5.10	0.66	1.27	0.00	2.03	0.98	0.33	0.66	0.34	1.31	0.00	0.99	0.00	1.66	0.34	1.00	0.00	0.65	0.32	0.00	0.00
Oxidized/Altered	37.80	15.54	13.27	21.85	27.62	30.03	51.01	19.93	26.67	29.57	37.29	31.80	24.20	44.37	28.42	30.79	30.98	29.24	37.86	35.18	41.23	19.32	32.12
Sillimanite	0.00	0.00	0.34	0.00	3.49	1.37	0.68	1.63	2.00	0.00	0.68	1.31	4.14	0.00	4.45	0.00	7.41	1.33	2.59	6.51	0.00	0.00	8.61
Tourmaline	3.09	4.05	8.84	0.66	2.54	1.02	0.00	0.65	0.67	1.00	2.03	0.98	0.96	0.33	3.77	0.00	0.00	1.00	2.27	0.00	0.00	0.68	0.00
Total	85.57	92.57	89.46	85.43	88.89	85.67	97.30	85.62	75.33	96.35	90.85	90.82	98.09	91.06	97.60	95.70	98.65	87.38	100.00	97.72	92.21	55.59	93.71

[illegible]

Mineral	FG	KG	BSG	GHIC	MVG
Andalusite			X		
Anthophyllite		X			
Apatite	X		X	X	
Augite, brown					X
Augite, green	X	X	X	X	
Augite, green/brown	X	X	X	X	
Augite, purple					X
Augite, red/pink	X	X	X	X	
Biotite		X		X	
Cassiterite				X	
Chlorite			X		
Clinozoisite		X	X		
Diopside	X	X	X	X	
Dolomite		X			
Enstatite	X				
Epidote		X	X		
Garnet		X	X	X	
Glass w/inclusions					X
Hornblende br					X
Hornblende gr/br		X		X	
Hypersthene	X				
Kyanite			X	X	
Monazite		X		X	
Muscovite		X			
Olivine	X				X
Opaque					
Rutile		X			
Serpentine	X				
Sillimanite			X		
Sphene/Titanite			X	X	
Staurolite			X		
Topaz				X	
Tourmaline			X	X	
Tremolite		X	X	X	
Zircon			X	X	

Table 3 – Comprehensive list of heavy minerals observed and their possible provenances. FG – Ferrar Group, KG – Koettlitz Group, BSG – Beacon Supergroup, GHIC – Granite Harbour Intrusive Complex, MVG – McMurdo Volcanic Group.